FINAL REPORT

PROJECT A-792

PANEL FLUTTER AERODYNAMICS

E. F. E. ZEYDEL

Contract NAS8-11396

25 June 1964 to 25 September 1965

Prepared for
George C. Marshall Space Flight Center
National Aeronautics and Space Administration
Huntsville, Alabama 35812

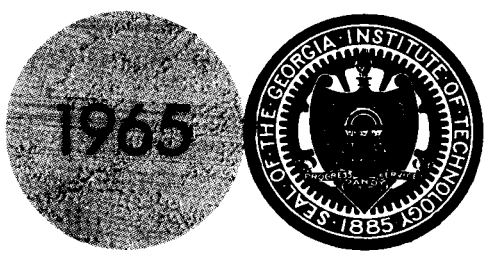

Engineering Experiment Station
GEORGIA INSTITUTE OF TECHNOLOGY
Atlanta, Georgia

GEORGIA INSTITUTE OF TECHNOLOGY
School of Aerospace Engineering
Atlanta, Georgia

FINAL REPORT

PROJECT A-792

PANEL FLUTTER AERODYNAMICS

By

E. F. E. Zeydel

CONTRACT NAS8-11396

25 JUNE 1964 to 25 SEPTEMBER 1965

Prepared for
GEORGE C. MARSHALL SPACE FLIGHT CENTER
NATIONAL AERONAUTICS AND SPACE ADMINISTRATION
HUNTSVILLE, ALABAMA

PREFACE

This report covers research initiated by the National Aeronautics and Space Administration, George C. Marshall Space Flight Center, Huntsville, Alabama, and performed under Contract No. NAS8-11396. The work was administered by Dr. M. F. Platzer of the Aeroballistics Laboratory.

The principal investigator of the program was Dr. E. F. E. Zeydel.

This report covers work done under this contract for the period June 25, 1964, to September 25, 1965.

The author wishes to acknowledge the contributions of Mr. L. Knight for the design of the probe mechanism and Professor A. C. Bruce, Mr. F. F. Rudder, and Mr. N. R. Maddox for their contributions in the supporting analysis for the model and probe design. Finally, the author would like to thank Mrs. Sue Bailey for the preparation of the manuscript.

ABSTRACT

16494

A new method for predicting in low supersonic flow the flutter boundaries for a very low aspect ratio rectangular flat panel is presented. The method is based on linearized, three-dimensional potential flow theory and small deflection plate theory. Only the simply supported edge condition has been considered, although other edge conditions can be treated in a similar manner.

An analysis for the determination of the model parameters of a stationary wavy wall wind tunnel model is given.

The design of a boundary layer probe to obtain adequate experimental information for the description of the velocity distribution and the pressure distribution within a turbulent boundary layer of variable thickness is also presented. The probe is sting supported and capable of traversing the boundary layer in three mutually perpendicular directions.

Author

TABLE OF CONTENTS

TABLE OF CONTENTS

List of Figures

LIST OF SYMBOLS

a = panel chord

$2b$ = panel span

c_∞ = speed of sound

D = $Eh^3/12(1-\nu^2)$ = flexural rigidity of panel

E = modulus of elasticity

g = structural damping coefficient

h = panel thickness

j^2 = -1

k = $\omega b/U$ = reduced frequency

M = Mach number

p_u = perturbation pressure at upper surface

q = $\rho U^2/2$ = dynamic pressure

R,S = defined by (7)

$\bar{R},\bar{S}$, = defined by (11)

r = wave number in the spanwise direction defined by (33)

s = $a/2b$ = $1/AR$ = inverse of aspect ratio of panel

t = time

U = freestream velocity

w = transverse displacement of panel (in the z-direction)

x,y,z= reference coordinate system

β = $(M^2-1)^{1/2}$

Γ = defined by (25)

γ = defined by (94)

δ = defined by (8)

ϵ = defined by (56)

λ = wave number in the chordwise direction defined by (33)

μ = $\tau\rho_s/\rho$

ν = Poisson's ratio

ρ = mass air density

ρ_s = mass density of panel

τ = h/b = non-dimensional panel thickness ratio

Φ = chordwise deflection function

φ = velocity potential

Ψ = spanwise deflection function

ω = frequency of vibration

$( )_\xi = \frac{\partial( )}{\partial\xi}$

$( )^*$ = Laplace transform of ( )

I. INTRODUCTION

In the development of design criteria to prevent the flutter of flat panels, panel geometries with very low aspect ratios are of particular interest in view of the panel configurations on the Saturn vehicle. For such geometries, very little information, either theoretical or experimental, is available particularly in the low supersonic region. The lack of adequate design criteria necessitates the development of new theories to supplement present information and to guide the proper design of experimental models.

In this report, a new method for predicting the flutter boundaries for a very low aspect ratio flat panel in low supersonic flow is presented. The method is based on linearized, three-dimensional potential flow theory and small deflection plate theory. In the analysis Laplace transform techniques are employed, which circumvent the need for introducing a large number of deformation functions such as in the Ritz-Galerkin method. Only the simply supported edge condition has been considered, although other edge conditions can be treated in a similar manner.

Stationary wavy wall type models with wave length comparable to the wave length of typical panel flutter modeshapes have been selected as the most suitable for gathering initial experimental information on the effects of a turbulent boundary layer on the pressure distribution of a flat oscillating panel in low supersonic flow. Of particular importance for the design of the models is the selection of a suitable amplitude to wave-length ratio. An analysis pertaining to this problem is given.

To investigate the effects of a turbulent boundary layer of variable thickness over the wavy wall model, a boundary layer probe extending from the sting support and capable of traversing the boundary layer in three mutually perpendicular directions was designed. Consideration was given to a probe design which allows accurate measurements of both total and static pressures in order to obtain adequate experimental information for a description of the velocity distribution and the pressure variation within the boundary layer. This instrumentation together with that of the wavy wall models, which supply the pressure distribution on the surface, should provide sufficient information for a comparison with available aerodynamic theories. The probe design and instrumentation are presented in this report.

II. PANEL FLUTTER SURVEY

A brief literature search was conducted to collect information on design criteria and available aerodynamic theories for the supersonic flutter of flat panels. The most recent information pertaining to this

problem is given in [1] - [14].* The reports specifically oriented towards design criteria are [3], [9], and [11]. The reports concerning new methods of analysis are [1], [2], [8], [10], [13], and [14]. Attempts to account for the effects of a turbulent boundary layer are given in [1] and [12]. In [4] - [7], a comparison between theory and experiment is made.

The only report dealing directly with the problem of particular interest here, the very low aspect ratio case, is that of Dowell [13]. Dowell makes the assumption that the panel has an infinite chord and treats the problem by means of the traveling wave solution of Miles [10]. He also postulates that for a panel whose length is long compared to the critical wave length (finite chord panel), his model should adequately describe, at least asymtotically, the true flutter boundary.

Theoretical and experimental results indicate, however, that the assumption of a flutter modeshape in the form of a traveling wave is not realistic for the finite chord panel even when the aspect ratio is very small. The flutter modeshapes usually found are increasing in amplitude towards the trailing edge of the panel. This certainly holds true for aspect ratios down to 1/10 [2]. Since this behavior is partly due to the reflection of the wave at the trailing edge (which the traveling wave solution neglects), there is no reason to expect that similar results will not be characteristic for aspect ratios of 1/60.

The most disturbing characteristic of the traveling wave solution is that flutter is predicted when the relative velocity between the forward velocity and wave velocity is subsonic. This is, of course, in direct contradiction to the more conventional panel flutter analysis, where the relative velocity must be supersonic in order to obtain flutter. In the ensuing section a method for solving the very low aspect ratio case has, therefore, been derived by extending the conventional supersonic panel flutter analysis.

III. THEORETICAL CONSIDERATIONS

A. Equations of Motion

Consider the uniform rectangular panel of finite chord, a, and finite span, $2b$, shown in Fig. 1, exposed to supersonic flow on the side $z > 0$. From small deflection plate theory, the equation of motion for the panel is [8,9]

$$D\nabla^4 w + \rho_s h w_{tt} + p_u = 0 \tag{1}$$

*Numbers in brackets refer to the bibliography.

In Eq. (1), w is the transverse displacement in the z-direction, D the plate bending stiffness, ρ_s the material density, h the plate thickness and p_u the aerodynamic pressure of the air flow at the side $z > 0$.

It is convenient to introduce dimensionless variables x' , y' , etc., by writing

$$x = bx' \quad ; \quad y = by'$$

$$w = bw' \quad ; \quad p_u = \rho U^2 p_u' \tag{2}$$

where ρ is the air density and U is the forward velocity.

Dropping the primes in the ensuing discussion, Eq. (1) in dimensionless form becomes

$$w_{4x} + 2w_{2x,2y} + w_{4y} + \frac{\rho_s h b^4}{D} w_{tt} + \frac{\rho U^2 b^3}{D} p_u = 0 \tag{3}$$

The panel boundaries in dimensionless form are at

$$x = 0 \quad ; \quad x = 2s$$

and

$$y = \pm 1 \tag{4}$$

where

$$s = a/2b$$

Since the motion at flutter is harmonic, we let

$$w(x,y,t) = \bar{w}(x,y)\, e^{j\omega t}$$

$$p_u(x,y,t) = \bar{p}_u(x,y)\, e^{j\omega t} \tag{5}$$

Substitution in (3) gives

$$\bar{w}_{4x} + 2\bar{w}_{2x,2y} + \bar{w}_{4y} + Rk^2\bar{w} + S\bar{p}_u = 0 \tag{6}$$

where

$$R = \frac{\rho_s h b^4 \omega^2}{Dk^2}$$

$$S = \frac{\rho U^2 b^3}{D} \tag{7}$$

and

$$k = \frac{\omega b}{U}$$

The parameters R and S can be written in terms of the more conventional panel flutter parameters

$$\mu = \frac{\tau \rho_s}{\rho}$$

and

$$\delta = \frac{\rho_s}{\rho}\left[\frac{q(1-\nu^2)}{E}\right]^{1/3} \tag{8}$$

where

$$\tau = \frac{h}{b}$$

E = modulus of elasticity

ν = Poisson's ratio

Since

$$D = \frac{Eh^3}{12(1-\nu^2)}$$

there follows from (7) and (8),

$$R = 24\,\frac{\delta^3}{\mu^2} = \mu S$$

and

$$S = 24\,\frac{\delta^3}{\mu^3} \tag{9}$$

In order to account for the effects of structural damping, the first three terms on the left-hand side of (6) are multiplied by $(1 + jg)$ and the equation of motion becomes

$$\bar{w}_{4x} + 2\bar{w}_{2x,2y} + \bar{w}_{4y} + \bar{R}k^2\bar{w} + \bar{S}\bar{p}_u = 0 \tag{10}$$

where

$$\bar{R} = \frac{R}{1+jg}$$

$$\bar{S} = \frac{S}{1+jg} \tag{11}$$

The panel flutter problem consists of finding for specific values of Mach number, M, structural damping, g, and inverse aspect ratio, $s = a/2b$ the particular combination of the parameters μ and δ which satisfies (10), together with (8), (9), (11), and the boundary conditions of the panel

configuration. The magnitude of this problem has led to the introduction of a variety of simplifying assumption mainly in the derivation of the aerodynamic pressure distribution. As a consequence, the majority of design criteria developed are restricted to either specific external flow conditions or assumed panel flutter behavior such as the traveling wave solutions.

Of particular interest in this report is the slender panel configuration with finite chord length and inverse aspect ratio in the order of 10 to 60. The configuration is exposed to low supersonic flow, which necessitates the use of linearized, three-dimensional aerodynamic theory.

An application of the Ritz-Galerkin method, whereby a suitable set of orthogonal deflection functions satisfying the boundary conditions are introduced, seems unjustified since it is to be expected that a large amount of generalized coordinates will be necessary for a satisfactory solution with inverse aspect ratios in the order of 10 to 60. In addition, the large amount of generalized coordinates will also lead to difficulties in computation to maintain accuracy.

The traveling wave solutions of Miles [10] and Dowell [13] are interesting, but they require the assumption that the panel chord is infinite so that no proper account of the reflections of the leading and trailing edge on the panel motion can be given. In addition, in the traveling wave solutions the flutter modeshape in the chordwise direction is specified at the onset of the analysis and the validity of this assumption can, therefore, only be verified by an analysis of a more general nature or by experimentation.

It is expected, however, that the proper representation of the deflections in the chordwise direction is more important than those in the spanwise direction since the direction of flow is in the chordwise direction. Similar to the procedure in [9], simplification has, therefore, been obtained by introducing a specific spanwise deflection function in the ensuing analysis.

Returning to the solution of Eq. (10), let

$$\bar{w} = A\Phi(x)\,\Psi(y) \tag{12}$$

An appropriate choice for the spanwise deflection function, $\Psi(y)$, is the modeshape associated with the lowest natural frequency of a beam with span $y = 2$. For simply supported side edges, $\Psi(y)$ becomes

$$\Psi(y) = \cos\frac{\pi}{2}y \quad ; \quad |y| \leq 1$$

$$\Psi(y) = 0 \quad ; \quad |y| > 1 \tag{13}$$

Substitution of (12) and (13) in (10) yields

$$A\left[\Phi_{4x} - 2\left(\frac{\pi}{2}\right)^2 \Phi_{2x} + \left(\frac{\pi}{2}\right)^4 \Phi + \bar{R}k^2\Phi\right] \cos\frac{\pi}{2} y + \bar{S}\bar{p} = 0 \quad ; \quad |y| \leq 1 \qquad (14)$$

Now, take the Laplace transform with respect to x. This gives, with the definitions

$$L[\Phi(x)] = \Phi^*(p)$$

$$L(\bar{p}_u) = \bar{p}_u^*(p) \qquad (15)$$

and the application of the simply supported boundary condition at $x = 0$ $[\Phi(0) = \Phi''(0) = 0]$,

$$A\left\{\left[\left(p^2 - \frac{\pi^2}{4}\right)^2 + \bar{R}k^2\right]\Phi^* - \left[p^2 - 2\left(\frac{\pi}{2}\right)^2\right]\Phi'(0) - \Phi'''(0)\right\} \cos\frac{\pi}{2} y$$

$$+ \bar{S}p_u^* = 0 \quad ; \quad |y| \leq 1 \qquad (16)$$

In (16), the primes denote differentiation with respect to x.

The Laplace transform and other approximations of the aerodynamic pressure distribution for panel flutter analysis will be defined in the next section.

B. Aerodynamic Pressure Distribution

1) The Laplace transform of the aerodynamic pressures. Since the region between Mach 1 and $\sqrt{2}$ is of particular interest, the aerodynamic pressures are obtained from linearized, three-dimensional aerodynamic theory.

The governing equation to be satisfied by the velocity potential, φ, is

$$(1-M^2)\varphi_{xx} + \varphi_{yy} + \varphi_{zz} = \frac{2M^2}{c_\infty}\varphi_{xt} + \frac{1}{c_\infty^2}\varphi_{tt} \qquad (17)$$

where M is the freestream Mach number and c_∞ is the speed of sound at infinity.

The boundary condition on φ is

$$\varphi_{z/z=0} = w_t + Uw_x \qquad (18)$$

The pressure at the upper surface in terms of φ is given by

$$p_u = -\rho(\varphi_t + U\varphi_x) \tag{19}$$

For convenience, we introduce again the dimensionless parameters of (2) and also

$$\varphi = bU\varphi' \tag{20}$$

and drop the primes in the ensuing discussion.

Since the motion at flutter is harmonic, let again

$$w(x,y,t) = \bar{w}(x,y)\, e^{j\omega t}$$

$$\varphi(x,y,t) = \bar{\varphi}(x,y)\, e^{j\omega t}$$

and

$$p_u(x,y,t) = \bar{p}_u(x,y)\, e^{j\omega t} \tag{21}$$

When

$$\bar{w}(x,y) = A\Phi(x) \cos ry \quad ; \quad -\infty < y < +\infty \tag{22}$$

we find from the analysis of Luke and St. John [14] that for supersonic flow the velocity potential satisfying (17) and (18) and the aerodynamic pressures can be written in the dimensionless forms

$$\bar{\varphi} = -\frac{A}{\beta} \cos ry \int_0^x (jk\Phi + \Phi_x)\, G(x-\xi)\, d\xi \quad ; \quad -\infty < y < +\infty \tag{23}$$

and

$$\bar{p}_u = -(jk\varphi + \varphi_x) \tag{24}$$

where

$$\beta = \sqrt{M^2-1}$$

$$G(x) = e^{-j\bar{\omega}x} J_o(\Gamma x)$$

$$\bar{\omega} = k\frac{M^2}{\beta^2}$$

$$\Gamma^2 = k^2\frac{M^2}{\beta^4} + \frac{r^2}{\beta^2} \tag{25}$$

Taking the Laplace transform with respect to x, yields, since $\bar{\varphi}(0) = \Phi(0) = 0$,

$$\bar{\varphi}^* = -\frac{A}{\beta} \cos ry \; (p + jk) \; \Phi^* \; G^* \tag{26}$$

and

$$\bar{p}_u^* = -(p+ jk) \; \bar{\varphi}^* \tag{27}$$

Now, the Laplace transform of G {see Eq. (25) and [15] pp. 236 (34)} is

$$G^* = [(p + j\bar{\omega})^2 + \Gamma^2]^{1/2} \tag{28}$$

Combining (26), (27), and (28), the Laplace transform of the aerodynamic pressures corresponding to (22) becomes

$$\bar{p}_u^* = \frac{A}{\beta} \cos ry \; \frac{(p+jk)^2}{[(p+j\bar{\omega})^2 + \Gamma^2]^{1/2}} \; \Phi^* \tag{29}$$

In order to obtain the Laplace transform of the aerodynamic pressures corresponding to the deflection functions

$$\bar{w} = A\Phi(x) \; \Psi(y) \tag{30}$$

where $\Psi(y)$ is given by (13), we represent $\Psi(y)$ in Fourier cosine integral form,

$$\Psi(y) = \int_0^\infty \frac{\cos r \cos ry}{(\pi^2/4)-r^2} \; dr \quad ; \quad -\infty < y < +\infty \tag{31}$$

Using (22), (29), and (31), the Laplace transform of the aerodynamic pressures corresponding to (30) becomes

$$\bar{p}_u^* = \frac{A}{\beta} \; (p+jk)^2 \int_0^\infty \frac{\cos r \cos ry \; dr}{[(\pi^2/4)-r^2][(p+j\omega)^2 + \Gamma^2]^{1/2}} \; \Phi^* \tag{32}$$

Because of the appearance of the Laplace transform variable p in the kernel of the integral, the expression (32) becomes rather unattractive for use in a panel flutter analysis. To study the flutter characteristics of very slender panels, the assumption has, therefore, been made that the pressure distribution at flutter can, with adequate accuracy, be described by using the approximation (29) for deflection functions of the form (30).

2) The aerodynamic pressures for wavy walls. The aerodynamic pressures on stationary or traveling wavy walls of infinite extent in the chord- and spanwise direction can be derived from the well-known Ackeret solution [16].

Let the stationary wavy wall boundary be given by

$$w = \mathrm{Re}(Ae^{i\lambda x} \cos ry) \tag{33}$$

The linearized equation for the velocity potential in a flow of Mach number M_1, above the wall is [see Eq. (17)]

$$(1-M_1^2)\varphi_{xx} + \varphi_{yy} + \varphi_{zz} = 0 \tag{34}$$

For flow to the right (i.e., in the positive x-direction), the boundary condition is

$$\varphi_z|_{z=0} = Uw_x$$

$$= M_1 c_\infty w_x \tag{35}$$

and the pressure perturbation at the wall is

$$p_u = -\rho M_1 c_\infty \varphi_x|_{z=0} \tag{36}$$

For flow to the left, the boundary condition is

$$\varphi_z|_{z=0} = -M_1 c_\infty w_x \tag{37}$$

and the pressure perturbation at the wall is

$$p_u = \rho M_1 c_\infty \varphi_x|_{z=0} \tag{38}$$

Let

$$\varphi = \mathrm{Re}[e^{i\lambda x} \cos ry\, h(z)] \tag{39}$$

To satisfy (34), $h(z)$ should satisfy

$$h_{zz} - [\lambda^2(1-M_1^2) + r^2]\, h = 0 \tag{40}$$

The general solution is

$$h = Be^{\alpha z} \tag{41}$$

where

$$\alpha = \pm [\lambda^2(1-M_1^2) + r^2]^{1/2} \tag{42}$$

The solution splits into cases

Case a:

$$\lambda^2(1-M_1^2) + r^2 > 0$$

or

$$M_1 < (1 + r^2/\lambda^2)^{1/2} \tag{43}$$

and

Case b:

$$\lambda^2(1-M_1^2) + r^2 < 0$$

or

$$M_1 > (1 + r^2/\lambda^2)^{1/2} \tag{44}$$

For $M_1 < (1 + r^2/\lambda^2)^{1/2}$, the solution of (40) which is finite at infinity gives

$$\varphi = \mathrm{Re}\left\{ Be^{i\lambda x} \cos ry\, e^{-|\lambda|\left[(1-M_1^2) + \frac{r^2}{\lambda^2}\right]^{1/2} z} \right\} \tag{45}$$

and from (35), for flow to the right

$$B = - \frac{iM_1 c_\infty \lambda A}{|\lambda|\left[(1-M_1^2) + \frac{r^2}{\lambda^2}\right]^{1/2}} \tag{46}$$

while from (37), for flow to the left

$$B = + \frac{iM_1 c_\infty \lambda A}{|\lambda|\left[(1-M_1^2) + \frac{r^2}{\lambda^2}\right]^{1/2}} \tag{47}$$

Using (36) and (38), there follows that for flow to the right or left

$$p_u = -\rho M_1^2 c_\infty^2 \mathrm{Re}\left\{\frac{|\lambda| A}{\left[(1-M_1^2) + \frac{r^2}{\lambda^2}\right]^{1/2}} e^{i\lambda x} \cos ry\right\} \tag{48}$$

For $M_1 > \left(1 + \frac{r^2}{\lambda^2}\right)^{1/2}$, the solution of (40) which satisfies the condition that there be no incoming disturbances from infinity yields

$$\varphi = \mathrm{Re}\left\{Ce^{i\lambda\left\{x - \left[(M^2-1) - \frac{r^2}{\lambda^2}\right]^{1/2} z\right\}} \cos ry\right\} \tag{49}$$

for flow to the right, and

$$\varphi = \mathrm{Re}\left\{Ce^{i\lambda\left\{x + \left[(M_1^2-1) - \frac{r^2}{\lambda^2}\right]^{1/2} z\right\}} \cos ry\right\} \tag{50}$$

for flow to the left.

Using (35) and (37),

$$C = -\frac{M_1 c_\infty A}{\left[(M_1^2-1) - \frac{r^2}{\lambda^2}\right]^{1/2}} \tag{51}$$

for flow to the left or right.

The pressure perturbation, from (36), is

$$p_u = \rho c_\infty^2 M_1^2 \mathrm{Re}\left\{\frac{i\lambda A}{\left[(M_1^2-1) - \frac{r^2}{\lambda^2}\right]^{1/2}} e^{i\lambda x} \cos ry\right\} \tag{52}$$

for flow to the right, while from (38),

$$p_u = -\rho c_\infty^2 M_1^2 \mathrm{Re}\left\{ \frac{i\lambda A}{\left[(M_1^2-1) - \frac{r^2}{\lambda^2} \right]^{1/2}} e^{i\lambda x} \cos ry \right\} \tag{53}$$

for flow to the left.

The aerodynamic pressures on a traveling wavy wall can readily be derived from the solution of the stationary wavy wall. Let the wavy wall boundary be given by

$$w = \mathrm{Re}\left[A e^{i\lambda\left(x + \frac{\omega}{\lambda} t\right)} \cos ry \right] \tag{54}$$

and the flow velocity above the wall in the positive x-direction be given by $U = Mc_\infty$. Clearly, (54) represents a traveling wave moving in the negative x-direction with velocity ω/λ.

Since the relative velocity between the flow and the wave is

$$U + \frac{\omega}{\lambda} = c_\infty\left(M + \frac{\omega}{\lambda c_\infty}\right)$$

the pressures on the traveling wave can be obtained from (48), (52), and (53) by substituting

$$M_1 = M + \frac{\omega}{\lambda c_\infty} \tag{55}$$

Defining

$$\epsilon = \sqrt{1 + \frac{r^2}{\lambda^2}} \tag{56}$$

we find that the aerodynamic pressures on the traveling wavy wall (33) become

$$p_u = \rho c_\infty^2 \mathrm{Re}\left[Q(M_1,\lambda,\epsilon)\, e^{i\lambda\left(x + \frac{\omega}{\lambda} t\right)} \cos ry \right] \tag{57}$$

where

$$Q(M_1,\lambda,\epsilon) = \frac{i\lambda M_1^2 A}{\left(M_1^2 - \epsilon^2\right)^{1/2}} \quad ; \quad M_1 > \epsilon$$

$$= -\frac{|\lambda| M_1^2 A}{\left(\epsilon^2 - M_1^2\right)^{1/2}} \quad ; \quad |M_1| < \epsilon$$

$$= -\frac{i\lambda M_1^2 A}{\left(M_1^2 - \epsilon^2\right)^{1/2}} \quad ; \quad M_1 < -\epsilon \tag{58}$$

The interesting case for the determination of panel flutter characteristics is the aerodynamic pressure distribution corresponding to a traveling wave which travels in the positive x-direction since waves traveling in the negative x-direction cannot be realized practically.

We, therefore, define the wavy wall boundary by

$$w = \mathrm{Re}\left(Ae^{-i\lambda x}\cos ry\, e^{i\omega t}\right) \tag{59}$$

where λ and r are considered positive.

The relative velocity between the flow and the wave has the Mach number

$$M_1 = M - \frac{\omega}{\lambda c_\infty} \tag{60}$$

which in the most practical cases may also be considered positive.

Following the derivation above, the aerodynamic pressures of practical importance corresponding to (59) are given by

$$p_u = \rho c_\infty{}^2 \mathrm{Re}\left[Q(M_1,\lambda,\epsilon)\, e^{-i\lambda x}\cos ry\, e^{i\omega t}\right] \tag{61}$$

where

$$Q(M_1,\lambda,\epsilon) = \frac{-i\lambda M_1{}^2 A}{\left(M_1{}^2 - \epsilon^2\right)^{1/2}} \quad ; \quad M_1 > \epsilon$$

$$= -\frac{\lambda M_1{}^2 A}{\left(\epsilon^2 - M_1{}^2\right)^{1/2}} \quad ; \quad M_1 < \epsilon$$

and

$$\epsilon = \sqrt{1 + \frac{r^2}{\lambda^2}} \tag{62}$$

Note that since M_1 as well as ϵ are taken to be positive, only two cases remain. Also, when the relative velocity is subsonic, $M_1 < 1$, so that M_1 is always smaller than ϵ. When the relative velocity is supersonic, however, $M_1 > 1$ and M_1 can be either greater or smaller than ϵ depending on the ratio r/λ. It will be seen that this is of considerable importance when a more general spanwise variation of the traveling wave is assumed.

We introduce, as before, dimensionless variables by writing

$$x = bx' \quad ; \quad y = by'$$

$$w = bw' \quad ; \quad p_u = \rho U^2 p_u'$$

$$A = bA' \quad ; \quad k = \omega b/U$$

$$\lambda = \frac{1}{b}\lambda' \quad ; \quad r = \frac{1}{b} r' \tag{63}$$

and drop the primes in the following discussion.

The aerodynamic pressures in dimensionless form corresponding to

$$w = \mathrm{Re}\left(A e^{-i\lambda x} \cos ry\, e^{i\omega t}\right) \tag{64}$$

then yields

$$p_u = \mathrm{Re}\left[Q(M,\lambda,k,r)\, e^{-i\lambda x} \cos ry\, e^{i\omega t}\right] \tag{65}$$

where

$$Q(M,\lambda,k,r) = -\frac{i\lambda\left(1 - \frac{k}{\lambda}\right)^2 A}{\left[M^2\left(1 - \frac{k}{\lambda}\right)^2 - \left(1 + \frac{r^2}{\lambda^2}\right)\right]^{1/2}} \quad ; \quad M\left(1 - \frac{k}{\lambda}\right) > \left(1 + \frac{r^2}{\lambda^2}\right)^{1/2}$$

$$= -\frac{\lambda\left(1 - \frac{k}{\lambda}\right)^2 A}{\left[\left(1 + \frac{r^2}{\lambda^2}\right) - M^2\left(1 - \frac{k}{\lambda}\right)^2\right]^{1/2}} \quad ; \quad M\left(1 - \frac{k}{\lambda}\right) < \left(1 + \frac{r^2}{\lambda^2}\right)^{1/2} \tag{66}$$

The aerodynamic pressures corresponding to the wave

$$w = \mathrm{Re}\left[A e^{-i\lambda x}\, \Psi(y)\, e^{i\omega t}\right] \tag{67}$$

where

$$\Psi(y) = \cos \frac{\pi}{2} y \quad ; \quad |y| \leq 1$$

$$= 0 \quad ; \quad |y| > 1 \tag{68}$$

can be obtained from (64) and (65) by applying (31).

There follows, if $M\left(1 - \frac{k}{\lambda}\right) < 1$,

$$p_u = \mathrm{Re}\left\{-A \int_0^{\infty} \frac{\lambda\left(1 - \frac{k}{\lambda}\right)^2 \cos r \cos ry \, dr}{\left[\left(1 + \frac{r^2}{\lambda^2}\right) - M^2\left(1 - \frac{k}{\lambda}\right)^2\right]^{1/2}\left(\frac{\pi^2}{4} - r^2\right)} \; e^{-i\lambda x} \, e^{i\omega t}\right\} \tag{69}$$

while, if $M\left(1 - \frac{k}{\lambda}\right) > 1$,

$$p_u = \mathrm{Re}\left\{\left[-A \int_0^{\bar{\gamma}} \frac{i\lambda\left(1 - \frac{k}{\lambda}\right)^2 \cos r \cos ry \, dr}{\left[M^2\left(1 - \frac{k}{\lambda}\right)^2 - \left(1 + \frac{r^2}{\lambda^2}\right)\right]^{1/2}\left(\frac{\pi^2}{4} - r^2\right)}\right.\right.$$

$$\left.\left. -A \int_{\bar{\gamma}}^{\infty} \frac{\lambda\left(1 - \frac{k}{\lambda}\right)^2 \cos r \cos ry \, dr}{\left[\left(1 + \frac{r^2}{\lambda^2}\right) - M^2\left(1 - \frac{k}{\lambda}\right)^2\right]^{1/2}\left(\frac{\pi^2}{4} - r^2\right)}\right] \; e^{-i\lambda x} \, e^{i\omega t}\right\} \tag{70}$$

where

$$\bar{\gamma} = \lambda\left[M^2\left(1 - \frac{k}{\lambda}\right)^2 - 1\right]^{1/2}$$

The expression (69) corresponds with those of Dowell in [13]. The separation of the integral in two parts as in (70) has not been performed in [13].

The dimensionless pressure distribution in supersonic flow corresponding to the stationary wavy wall,

$$w = A \sin \lambda x \, \Psi(y) \tag{71}$$

follows directly from (70) by substituting, $M > 1$ and $k = 0$, thus

$$p_u = A\lambda^2 \left[\int_0^{\lambda\beta} \frac{\cos r \cos ry \, dr}{\left(\frac{\pi^2}{4} - r^2\right)\left(\lambda^2\beta^2 - r^2\right)^{1/2}} \cos \lambda x \right.$$

$$\left. - \int_{\lambda\beta}^{\infty} \frac{\cos r \cos ry \, dr}{\left(\frac{\pi^2}{4} - r^2\right)\left(r^2 - \lambda^2\beta^2\right)^{1/2}} \sin \lambda x \right] \tag{72}$$

where

$$\beta = \sqrt{M^2 - 1}$$

The aerodynamic pressures in subsonic flow, $M < 1$, corresponding to (71) are obtained from (69),

$$p_u = -A\lambda^2 \int_0^{\infty} \frac{\cos r \cos ry \, dr}{\left(\frac{\pi^2}{4} - r^2\right)\left(r^2 - \lambda^2\beta^2\right)^{1/2}} \sin \lambda x \tag{73}$$

The expressions (72) and (73) can be used for estimating the pressure distribution away from the leading edge on the three-dimensional wavy wall models to be tested at the National Aeronautics and Space Administration, Ames Research Center.

IV. SOLUTION OF PANEL FLUTTER EQUATIONS

Utilizing the approximation (29) with $r = \pi/2$ for the Laplace transform of the aerodynamic pressures, the Laplace transform of the flutter equations of motion are obtained by combining (16) and (29),

$$A \left\{ \left[\left(p^2 - \frac{\pi^2}{4}\right)^2 + \bar{R}k^2 + \bar{S} \frac{(p + jk)^2}{\beta\left[(p + j\bar{\omega})^2 + \Gamma^2\right]^{1/2}} \right] \Phi^* \right.$$

$$\left. - \left[p^2 - 2\left(\frac{\pi}{2}\right)^2\right] \Phi'(0) - \Phi'''(0) \right\} \cos \frac{\pi}{2} y = 0 \tag{74}$$

Consequently,

$$\Phi^* = \frac{A_1\Phi'(0) + \Phi'''(0)}{A_2 + A_3A_4^{-1}} \tag{75}$$

where

$$A_1(p) = p^2 - 2\left(\frac{\pi}{2}\right)^2$$

$$A_2(p) = \left(p^2 - \frac{\pi^2}{4}\right)^2 - \bar{R}k^2$$

$$A_3(p) = \bar{S}\,\frac{1}{\bar{\beta}}\,(p + jk)^2$$

$$A_4(p) = \left[(p + i\bar{\omega})^2 + \Gamma^2\right]^{1/2} \tag{76}$$

To obtain the inverse Laplace transform of Φ^*, we write (75) in the more convenient form

$$\Phi^* = \frac{\left(B_1 + B_2A_4^{-1}\right)\Phi'(0) + \left(B_3 + B_4A_4^{-1}\right)\Phi'''(0)}{C} \tag{77}$$

where

$$B_1(p) = A_1A_2A_4^2$$

$$B_2(p) = -A_1A_3A_4^2$$

$$B_3(p) = A_2A_4^2$$

$$B_4(p) = -A_3A_4^2$$

and

$$C(p) = A_2^2A_4^2 - A_3^2 \tag{78}$$

We assume that $C(p)$ has ten distinct complex roots, p_r, $(r = 1,2,\ldots 10)$, so that [see (75)]

$$L^{-1}\left(\frac{B_1 + B_2A_4^{-1}}{C}\right) = \sum_{r=1}^{10} \frac{B_1(p_r)}{C'(p_r)} e^{p_r x} + \sum_{r=1}^{10} \frac{B_2(p_r)}{C'(p_r)} \int_0^x e^{p_r(x-\xi)} e^{-i\bar{\omega}\xi} J_0(\Gamma\xi)\, d\xi$$

$$= D_1(x) \tag{79}$$

and

$$L^{-1}\left(\frac{B_3 + B_4A_4^{-1}}{C}\right) = \sum_{r=1}^{10} \frac{B_3(p_r)}{C'(p_r)} e^{p_r x} + \sum_{r=1}^{10} \frac{B_4(p_r)}{C'(p_r)} \int_0^x e^{p_r(x-\xi)} e^{-i\bar{\omega}\xi} J_0(\Gamma\xi)\, d\xi$$

$$= D_2(x) \tag{80}$$

Thus,

$$\Phi(x) = D_1(x)\Phi'(0) + D_2(x)\Phi'''(0) \tag{81}$$

To satisfy boundary conditions at the trailing edge of the panel, we will also need $\Phi''(x)$. Although this quantity can readily be obtained by differentiating (81), a more convenient form is obtained by writing

$$(\bar{\Phi}'')^* = \frac{p^2A_1\bar{\Phi}'(0) + p^2\bar{\Phi}'''(0)}{A_2 + A_3A_4^{-1}} - \bar{\Phi}'(0) \tag{82}$$

Let

$$A_5 = -\left(\frac{\pi}{2}\right)^4 + \bar{R}k^2$$

$$A_6 = p^2 \tag{83}$$

Using (76), there follows

$$(\bar{\Phi}'')^* = \frac{(A_5 - A_3A_4^{-1})\bar{\Phi}'(0) + A_6\bar{\Phi}'''(0)}{A_2 + A_3A_4^{-1}} \tag{84}$$

and thus

$$(\Phi'')^* = \frac{(B_5 + B_6 A_4^{-1})\Phi'(0) + (B_7 + B_8 A_4^{-1})\Phi'''(0)}{C} \tag{85}$$

where

$$B_5(p) = A_2 A_5 A_4^2 + A_3^2$$

$$B_6(p) = -(A_2 A_3 + A_3 A_5) A_4^2$$

$$B_7(p) = A_2 A_6 A_4^2$$

$$B_8(p) = -A_3 A_6 A_4^2 \tag{86}$$

and finally,

$$\Phi''(x) = D_3(x)\Phi'(0) + D_4(x)\Phi'''(0) \tag{87}$$

where

$$D_3(x) = \sum_{r=1}^{10} \frac{B_5(p_r)}{C'(p_r)} e^{p_r x} + \sum_{r=1}^{10} \frac{B_6(p_r)}{C'(p_r)} \int_0^x e^{p_r(x-\xi)} e^{-j\bar{\omega}\xi} J_o(\Gamma\xi)\, d\xi \tag{88}$$

and

$$D_4(x) = \sum_{r=1}^{10} \frac{B_7(p_r)}{C'(p_r)} e^{p_r x} + \sum_{r=1}^{10} \frac{B_8(p_r)}{C'(p_r)} \int_0^x e^{p_r(x-\xi)} e^{-j\bar{\omega}\xi} J_o(\Gamma\xi)\, d\xi \tag{89}$$

The flutter condition is obtained by satisfying the boundary conditions at the trailing edge of the panel. For the simply supported trailing edge, we must have

$$w = w'' = 0 \quad \text{at} \quad x = 2s \tag{90}$$

or

$$\Phi(2s) = \Phi''(2s) = 0 \tag{91}$$

The flutter condition follows from (81), (87), and (91),

$$E = E_R + jE_I = D_1(2s)D_4(2s) - D_2(2s)D_3(2s) = 0 \qquad (92)$$

The solution consists of a trail-and-error procedure. To satisfy (92), μ and k are chosen to be free parameters. For given values of M, g, δ, and s, μ and k are varied until both E_R and E_I are zero. The procedure is then repeated for different s. Flutter boundaries in the μ - s plane can thus be obtained for specific values of M, g, and δ.

Although not presented here, the clamped leading and trailing edge condition can be treated similarly.

To facilitate numerical evaluation, the expressions (79)-(81) and (87)-(92) have been written in a slightly different form. Since it is the objective of this program to obtain flutter boundaries for small aspect ratio panels ($s \gg 1$), the terms e^{pr^x} in the Eqs. (79), (80), (88), and (89) become large when $Re(p_r)$ is positive and large. This could cause overflow in the computer. To circumvent this difficulty, we order the roots, p_r, with respect to their real parts in the following way.

$$Re(p_1) > Re(p_2) > \ldots > Re(p_i) \geq 0 > Re(p_{i+1}) > \ldots > Re(p_{10}) \qquad (93)$$

and let

$$Re(p_1) = \gamma \qquad (94)$$

Next, let

$$\Phi(x) = e^{\gamma x}\left[\bar{D}_1(x)\Phi'(0) + \bar{D}_2(x)\Phi'''(0)\right] \qquad (95)$$

and

$$\Phi''(x) = e^{\gamma x}\left[\bar{D}_3(x)\Phi'(0) + \bar{D}_4(x)\Phi'''(0)\right] \qquad (96)$$

Since

$$e^{-\gamma x}\int_0^x e^{p_r(x-\xi)}e^{-i\bar{\omega}\xi}J_o(\Gamma\xi)\,d\xi = e^{(p_r-\gamma)x}\int_0^x e^{-(p_r+i\bar{\omega})\xi}J_o(\Gamma\xi)\,d\xi$$

$$= e^{-\gamma x}\int_0^x e^{p_r\xi}e^{-i\bar{\omega}(x-\xi)}J_o[\Gamma(x-\xi)]\,d\xi \qquad (97)$$

$\bar{D}_1(x)$-$\bar{D}_4(x)$ are given by the following expression,

$$\bar{D}_n(x) = \sum_{r=1}^{10} \frac{B_{2n-1}(p_r)}{C'(p_r)} e^{(p_r-\gamma)x} + \sum_{r=1}^{i} \frac{B_{2n}(p_r)}{C'(p_r)} e^{(p_r-\gamma)x} \int_0^x e^{-(p_r+i\bar{\omega})\xi} J_o(\Gamma\xi)\, d\xi$$

$$+ \sum_{r=i+1}^{10} \frac{B_{2n}(p_r)}{C'(p_r)} e^{-\gamma x} \int_0^x e^{p_r\xi} e^{-i\bar{\omega}(x-\xi)} J_o[\Gamma(x-\xi)]\, d\xi \quad ; \quad n = 1,2,3,4 \tag{98}$$

Note that in (98) the upper limit of the exponential terms is 1.

The flutter condition becomes

$$\bar{E} = \bar{E}_R + j\bar{E}_I = \bar{D}_1(2s)\bar{D}_4(2s) - \bar{D}_2(2s)\bar{D}_3(2s) = 0 \tag{99}$$

V. NUMERICAL RESULTS AND DISCUSSION

During the course of this research program an attempt has been made to obtain numerical results for the very low aspect ratio cases. The complexity of the flutter equations and the limited amount of time available has prevented the completion of these efforts.

At present, it is believed that the debugging of the computer program for the Burrough's B-5500 has been completed. To gain confidence in the program, a comparison with previously derived results [2] for $M = 1.35$, $g = .01$, $\delta = 22.738$, and $s = \frac{1}{4}$ (aspect ratio = 4) has been made. This comparison indicated a discrepency of 30 per cent in μ, although similar μ-k diagrams as previously derived were obtained. Initially, it was thought that further debugging in the computer program was necessary. However, the sensitivity of the panel flutter boundary to small changes in the low supersonic region and the application of a more precise method of analysis could also have caused the discrepency. It has, therefore, been concluded that a more extensive verification of results is required. Since such a verification is beyond the scope of the present project, it is proposed to continue this work under Contract NAS8-20100 titled, "Experimental Research on Panel Flutter Aerodynamics."

VI. MODEL AND BOUNDARY LAYER PROBE DESIGN

Stationary wavy wall type models with wave length comparable to the wave length of typical panel flutter modeshapes have been selected as the most suitable for gathering initial experimental information on the effects of a turbulent boundary layer on a flat oscillating panel in low supersonic flow.

The determination of model parameters and the design of a boundary layer probe are given in the next sections.

A. Determination of Wavy Wall Model Parameters

It is desired to estimate the wave parameter ϵ/ℓ (see figure) for a stationary wavy wall model which will exhibit measurable pressure differences referenced to free stream with deviations of the order of five per cent or less from linear aerodynamic theory. The dependence of the pressure difference and its deviation on the wave parameter is explicitly defined for two-dimensional supersonic flow by the following extension of linearized theory.

Assuming the panel model is defined by a sinusoidal wave with amplitude ϵ and wave length ℓ,

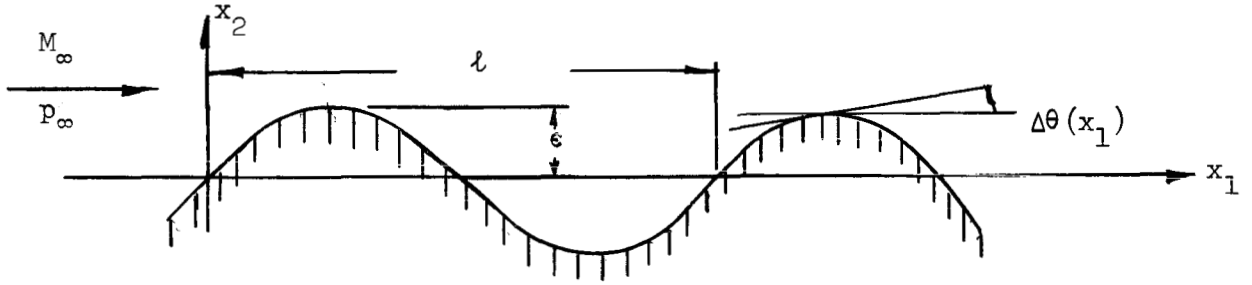

the equation for the wall is given by

$$x_2 = \epsilon \sin\left(\frac{2\pi}{\ell} x_1\right) \tag{100}$$

with local slope

$$\Delta\theta(x_1) = \frac{dx_2}{dx_1} = \frac{2\pi\epsilon}{\ell} \cos\left(\frac{2\pi}{\ell} x_1\right) \tag{101}$$

Now, using the characteristic relation for isentropic waves [17],

$$\pm\theta = \sqrt{\left(\frac{\gamma+1}{\gamma-1}\right)}\tan^{-1}\left\{\sqrt{\left[\frac{\gamma-1}{\gamma+1}\left(M^2-1\right)\right]}\right\} - \tan^{-1}\left[\sqrt{\left(M^2-1\right)}\right] + \text{const} \qquad (102)$$

and the isentropic flow relation

$$\frac{p_o}{p} = \left(1 + \frac{\gamma-1}{2}M^2\right)^{\frac{\gamma}{\gamma-1}} \qquad (103)$$

One may eliminate M and expand $(p - p_\infty)$ in terms of M_∞ and $\Delta\theta$, where M_∞ and p_∞ are the free-stream Mach number and pressure, respectively, γ is the ratio of specific heats, and $\Delta\theta$ is the turning angle of the local flow from the free-stream direction. The resulting series expansion of the dimensionless pressure difference is

$$\frac{p-p_\infty}{\frac{1}{2}\gamma p_\infty M_\infty^2} = C_1(\Delta\theta) + C_2(\Delta\theta)^2 + C_3(\Delta\theta)^3 + \ldots. \qquad (104)$$

with $\Delta\theta$ positive when measured counterclockwise from the free-stream flow direction. The coefficients are given as:

$$C_1 = \frac{2}{\sqrt{\left(M_\infty^2 - 1\right)}}$$

$$C_2 = \frac{\left(M_\infty^2 - 2\right)^2 + \gamma M_\infty^4}{2\left(M_\infty^2 - 1\right)^2}$$

$$C_3 = \frac{M_\infty^4}{\left(M_\infty^2 - 1\right)^{7/2}}\left[\frac{\gamma+1}{6}\left(M_\infty^2 - \frac{5 + 7\gamma - 2\gamma^2}{2(\gamma+1)}\right)^2\right.$$

$$\left. + \frac{-4\gamma^4 + 28\gamma^3 + 11\gamma^2 - 8\gamma - 3}{24(\gamma+1)}\right]$$

$$+ \frac{3\left(M_\infty^2 - 4/3\right)^2}{4\left(M_\infty^2 - 1\right)^{7/2}} \qquad (105)$$

The linear or first order approximation of $\frac{\Delta p}{p_\infty}$ is defined then as

$$\left(\frac{\Delta p}{p_\infty}\right)_1 = \tfrac{1}{2}\gamma M_\infty^2 C_1(\Delta\theta) \tag{106}$$

and the second order approximation as

$$\left(\frac{\Delta p}{p_\infty}\right)_2 = \tfrac{1}{2}\gamma M_\infty^2 \left[C_1(\Delta\theta) + C_2(\Delta\theta)^2\right] \tag{107}$$

The deviation of the second order approximation from the first is defined by

$$e = \frac{\left(\frac{\Delta p}{p_\infty}\right)_2 - \left(\frac{\Delta p}{p_\infty}\right)_1}{\left(\frac{\Delta p}{p_\infty}\right)_1} \tag{108}$$

so that

$$|e_{max}| = \frac{C_2}{C_1} |\Delta\theta_{max}| \tag{109}$$

It follows from the definition of the local slope that

$$|\Delta\theta_{max}| = \frac{2\pi\epsilon}{\ell} \tag{110}$$

corresponding to $x_1 = 0 , \frac{\ell}{2} , \ell , \ldots$ The maximum deviation is then given as

$$|e_{max}| = 2\pi \frac{C_2}{C_1} \frac{\epsilon}{\ell} \tag{111}$$

For air $(\gamma = 1.4)$ the maximum pressure difference according to the linear theory

$$\left|\left(\frac{\Delta p}{p_\infty}\right)_1\right|_{max} = \pi\gamma M_\infty^2 C_1 \frac{\epsilon}{\ell} \tag{112}$$

and the maximum deviation $|e_{max}|$ are computed for values of Mach number

in the low supersonic range and values of the wave parameter,

$$10^{-3} \leq \epsilon/\ell \leq 10^{-2}$$

The results, which are shown in Fig. 2, indicate that at M = 1.35 (the Mach number critical from a panel flutter point of view) the wave parameter ϵ/ℓ should be approximately 5×10^{-3} for a five per cent deviation in pressure from linear theory. The corresponding values of $\left|(\Delta p/p_\infty)_1\right|_{max}$ are of the order of 0.10 which should be adequate for accurate measurement.

B. Probe Design

1) Mechanism. The following discussion concerns the design of a probe (Fig. 3) for the two-foot transonic wind tunnel at the National Aeronautics and Space Administration, Ames Research Center, to measure the pressure distributions along wavy-wall models. The probe is capable of moving in three mutually perpendicular directions with the two movements parallel to the model manually controlled, and the movement perpendicular to the model automatically controlled by a computer which is presently in use at Ames. The desired maximum cross-sectional area of the probe is 1.5 per cent of the test section cross-sectional area. However, because of problems in the structural integrity of the probe mechanism, it was necessary to increase this figure to 1.525 per cent. An area chart appears as Fig. 4.

The general configuration of the probe mechanism is dictated by tunnel, aerodynamic, and mechanical design considerations. To meet tunnel and aerodynamic requirements, all tubular sections are terminated in cones and all other sections in wedges with maximum included angles of 16 degrees. Since the cross-sectional area is limited and the strength of the probe can only be increased either by increasing the cross-sectional area or by increasing the chord lengths of the aerodynamic surfaces (which results in higher lift) a compromise with respect to the safety factors for yield and ultimate stress had to be made. A stress analysis of the entire mechanism appears in a subsequent section of this report.

Extreme fabrication difficulties are presented in machining longitudinal holes in the solid wedge struts and in machining wedge shapes to slide inside other wedge shapes. Each of the wedge sections will, therefore, be fabricated in two sections and joined after machining with silver braze alloy Easy-Flo 45. To obtain maximum strength and obvivate corrosion difficulties the material chosen for these sections was 17-4 PH stainless steel. Since the hardening temperature for this material is 1150°F, and the braze alloy chosen has a flow temperature of 1125°F, the hardening and joining processes can be combined. Complete drawings of the probe mechanism will be furnished under NASA Contract No. NAS8-20100.

All movements of the probe are accomplished by means of D.C. motors, with suitable gear reductions, located in open-loop electrical control circuits. The magnitude of motion of any of the three probe movements is

controlled by the duration of an electrical pulse to the drive motor. Thus, no means are available for moving the probe to a predetermined position. However, each drive unit is attached to a potentiometer which accurately reflects the position of the probe at any point within the range of travel of the probe.

The probe is capable of a total of 60 inches of travel in the direction of the tunnel axis. This travel is accomplished in ten discrete, six-inch intervals. Within each six-inch interval, the probe motion is accomplished by an open-loop, direct-current drive motor and position potentiometer as discussed above. Vertical and horizontal motion, with respect to the tunnel axis, is limited to three inches, again accomplished by open-loop, direct-current motors and position potentiometers.

a) Outboard strut and motor pod. Fig. 5 presents a sketch of the outboard strut and motor pod. The motor pod has been sectioned to show the drive and potentiometer assembly as well as the pressure transducer location. The drive system for the moveable portion of the outboard struts consists of a .015 horsepower, 16,000 rpm, 28-volt D.C. motor and gear train which drives, through a worm gear, a 5-40 screw which, in turn, drives the strut. The motor reduction ratio through the worm gear is 20:1. Thus, for one complete turn of the motor the strut moves $1/20 \times 40 = 0.00125$ inches. Since the maximum speed of the motor is 16,000 rpm, the maximum translational speed of the moveable strut will be 0.33 inches/second. However, since the motor requires a finite time to come up to speed, the actual translational velocity of the strut will depend on the duration of the energizing pulse. It is anticipated that the average translational velocity for short pulses will probably be 0.1 inches/second, which should be compatible with the system presently in use at Ames.

The position indicator is a 1000 ohm, 10-turn potentiometer manufactured by the Spectrol Electronics Corporation of San Gabriel, California. The potentiometer is geared to the motor through a 306:1 reduction; therefore, for 0.001-inch translational movement of the strut, the potentiometer turns through 0.94 degrees or 0.277 ohms. The resolution of the potentiometer is 0.052 per cent or 0.52 ohms; thus, the position of the probe in the direction perpendicular to the model can be measured at best to $\pm$0.002 inches. Since the total movement of the strut is three inches, the potentiometer turns through 9.4 turns or 940 ohms for maximum extension.

The transducer has been located in the forward end of the motor pod to reduce the length of the pressure tubing. From this point, it is necessary to carry only the transducer wiring and the reference pressure tube through the mechanism to the recorder. Also, since both static and total pressure probes will be used, it becomes necessary that the transducer be so installed as to facilitate easy removal and replacement. As shown in Fig. 5, this can be accomplished by removing the threaded cone tip, breaking the wiring and pressure connections, and removing the transducer. The pressure-sensitive face of the transducer is sealed from all except the probe pressure by a gasketed cup held in place by an adjustable screw located in the cone tip.

Both the moveable and the fixed portions of the strut are diamond shaped. The moveable strut is closely fitted to the bottom side of the internal diamond of the fixed strut. The top side of the moveable strut is keyed by means of a 1/16 inch square key into the fixed strut to prevent binding under aerodynamic drag loads. The fixed strut is joined to the motor pod by means of a silver alloy braze joint on both sides of the pod.

b) Inboard strut and motor pod. Fig. 6 presents a sectional sketch of the inboard strut and motor pod. As shown, the motor pod is the terminal portion of the cylindrical sting of the mechanism. The maximum travel of the moveable portion of the strut is the same as for the outboard strut, three inches. The drive train is similar except that the motor-to-strut screw reduction is 40:1, the motor to potentiometer reduction is 400:1, and the strut is driven by an 8-32 screw. Thus, for 0.001-inch slider movement, the position potentiometer turns through 1.152 degrees or 0.319 ohms. Since the potentiometer resolution is the same as for the outboard strut, the position of the probe in this direction can be determined to be at best $\pm$0.00163 inches.

The strut is similar in construction to the outboard strut except that for additional strength the thickness is increased and a rectangular section is added between the leading and trailing wedges. Friction reduction is obtained by mating 1/16 inch x 0.950 inch surfaces on the top and bottom of the moveable strut to machined grooves in the inside of the fixed strut. Axial holes are provided in the moveable strut for the necessary wires and reference pressure tubes. The free end of the moveable strut is attached to the outboard strut motor pod by means of a silver alloy braze joint reinforced with four 1/16 inch pins. The fixed strut is mounted in the motor pod in the same manner as the outboard strut.

c) Axial motion actuator. Motion of the outboard strut-motor pod and inboard strut-motor-pod assembly in the axial direction of the tunnel is accomplished by two means. Nine discrete steps of six inches each of the entire sting-strut assembly are possible for rough positioning. For fine positioning in any six-inch interval, motion of the strut-motor-pod assembly is accomplished by driving this assembly with a D.C. motor through a 100:1 gear reduction by means of a 1/16 inch ball screw. A reducer has been placed between the motor and the potentiometer with a reduction ratio of 1092.37:1. Since the ball screw lead is 0.062 inches/turn and the potentiometer resolution is 0.052 per cent, positioning accuracy can possibly be $\pm$.0035 inches. Radial motion of the assembly is prevented by 1 inch x 1/4 inch keys mated to the inboard strut motor pod housing and the sting.

The discrete steps of the unit are accomplished by driving the entire sting-strut assembly, again by means of a D.C. motor and ball screws, through the sting support cylinder shown in Fig. 3. The intervals are controlled by fixing a micro-switch to the sting tube and locating circuit breakers at precise six-inch intervals. In order to drive the unit over the circuit breakers, a parallel switch is available which, when closed, furnishes power to the drive motor until the main circuit again closes. A schematic of the electrical circuitry appears in Fig. 7. The sting-strut assembly is supported in the sting-support tube by means of 12 rollers fixed to the sting support and rolling grooves machined into the outer surface of the sting tube as shown in the figure.

2) Structural integrity.

a) Aerodynamic loads. It is assumed for the purpose of calculating aerodynamic loads that the boundary layer probe support structure will be subjected to a dynamic pressure of 1800 psf in the low supersonic Mach number range. Estimates are given for the lift and drag distribution on the component parts of the structure, which for this purpose is considered to be made up of the following parts illustrated in Fig. 8.

Part	Name	c, chord	ℓ, span	t, thickness
0-1	Outboard section of outboard wing	1.556"	5.212"	0.219"
1-2	Inboard section of outboard wing	2.75"	6.00"	0.372"
2-3	Pod	16.00"	(DIA = 1.75")	
3-4	Outboard section of inboard wing	2.40"	3.125"	0.246"
4-5	Inboard section of inboard wing	4.00"	6.21"	0.500"

Further, for prediction of the aerodynamic coefficient, the wing sections are assumed to be symmetrical diamond airfoils with total apex angles of 16° and thickness ratios of 0.125.

Griffith [18] presents drag results obtained from theory and experiment for a 15° wedge with straight afterbody obtained in a shock tunnel and wind tunnel results for a 14.4° diamond due to Liepmann and Bryson [19]. These results together with those of similar wedge sections with varying thickness ratios, indicate that a value for the wing section drag coefficient may be chosen conservatively as

$$c_D = 0.09$$

Guderley and Yoshihara [20] present results for the slope of the lift curve for thin symmetrical diamond sections. Likewise, Vincenti, Dugan, and Phelps [21] plot results of theory and experiment for a thin, doubly symmetric wedge of approximately eight per cent thickness. From these results, it is concluded that a fair approximation to the lift curve slope for the wing sections is given by

$$\frac{dc_L}{d\alpha} = 5$$

While the drag load on the pod has been deemed insignificant in the stress analysis, its order of magnitude is of interest for loading deflection calculations. The results of Drougge [22] indicate that a reasonable value for this drag may be given by

$$c_{D_{pod}} = 0.2$$

based on frontal area.

Other aerodynamic coefficients are deemed of small effect or are inconsequential in a stress analysis of the boundary layer probe support.

Based upon the preceding aerodynamic coefficients, the loadings imposed on the component parts of the probe support are computed as follows:

Wing sections:

drag:

$$c_D = 0.09$$

$$D = \frac{c_D q_{max}}{12} (c") \ \#/ft.$$

$$w_D = \frac{D}{12} \ \#/in. \text{ of span}$$

where $q_{max} = 1800 \ \#/ft.^2$.

lift:

$$\frac{dc_L}{d\alpha} = 5$$

$$L = \frac{dc_L}{d\alpha} \frac{q_{max}}{12} (c") \frac{\alpha}{57.3} \ \#/ft.$$

$$w_L = \frac{L}{12} \ \#/in. \text{ of span}$$

where $q_{max} = 1800 \ \#/ft.^2$.

The load distributions thus produced are tabulated in the following table.

Part	w_D, drag load	w_L, lift load
0-1	1.75 #/in.	5.09 #/in.
1-2	3.09 #/in.	8.99 #/in.
3-4	2.70 #/in.	7.85 #/in.
4-5	4.50 #/in.	13.33 #/in.

Pod drag:

$$c_D = 0.2$$

$$D = c_D q_{max} A_f$$

where

$$q_{max} = 1800 \text{ \#/ft.}^2$$

and

$$A_f = 0.0167 \text{ ft.}^2$$

$$D = 6.01 \text{ \#}$$

b) Stress analysis and test. The aerodynamic loads section tabulates load distributions for the boundary layer probe support subjected to a dynamic pressure of 1800 psf and a three degree angle-of-attack for both inboard and outboard struts.

The distributions were found to be as follows:

Part	Name	w_D, drag load	w_L, lift load
0-1	Outboard section of outboard strut	1.75 #/in.	5.09 #/in.
1-2	Inboard section of outboard strut	3.09 #/in.	8.99 #/in.
2-3	Pod	6.01 #	
3-4	Outboard section of inboard strut	2.70 #/in.	7.85 #/in.
4-5	Inboard section of inboard strut	4.50 #/in.	13.33 #/in.

These loadings are shown on the boundary layer probe support in Fig. 8.

Free-body diagrams of the sections of the boundary layer probe support are as follows:

Section (0-1).

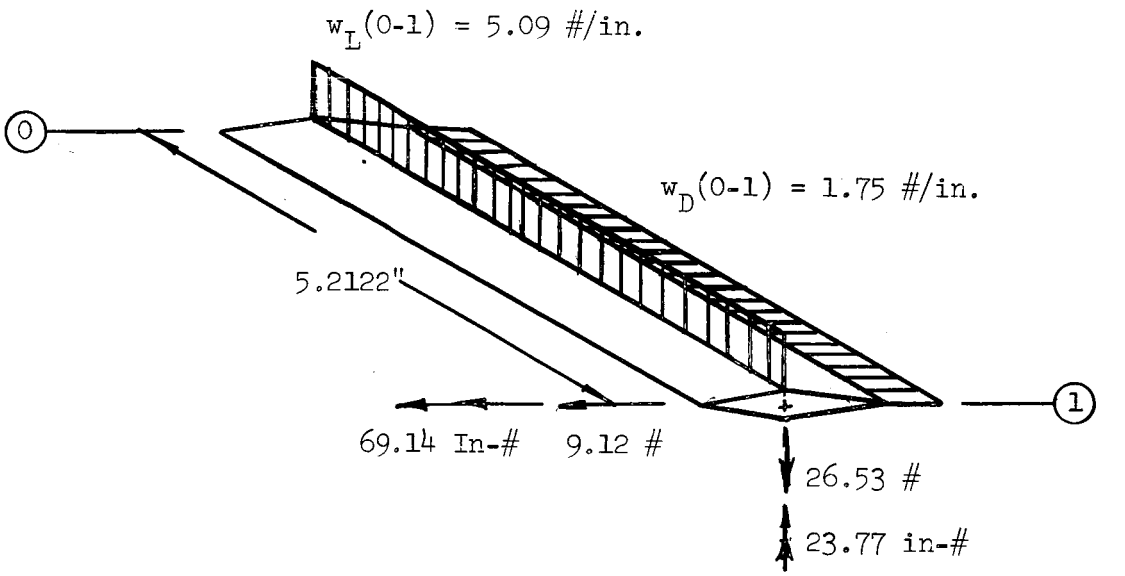

Section (1-2).

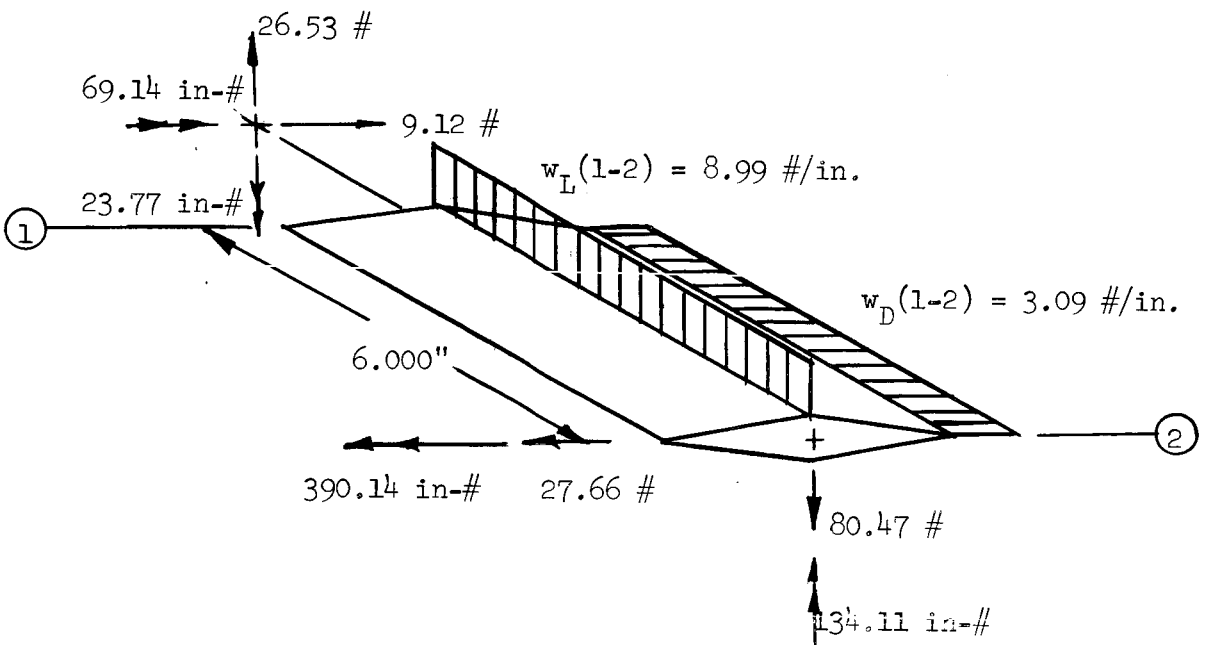
26.53 #
69.14 in-#
9.12 #
23.77 in-#
1
w_L(1-2) = 8.99 #/in.
w_D(1-2) = 3.09 #/in.
6.000"
2
390.14 in-#
27.66 #
80.47 #
134.11 in-#

Section (2-3).

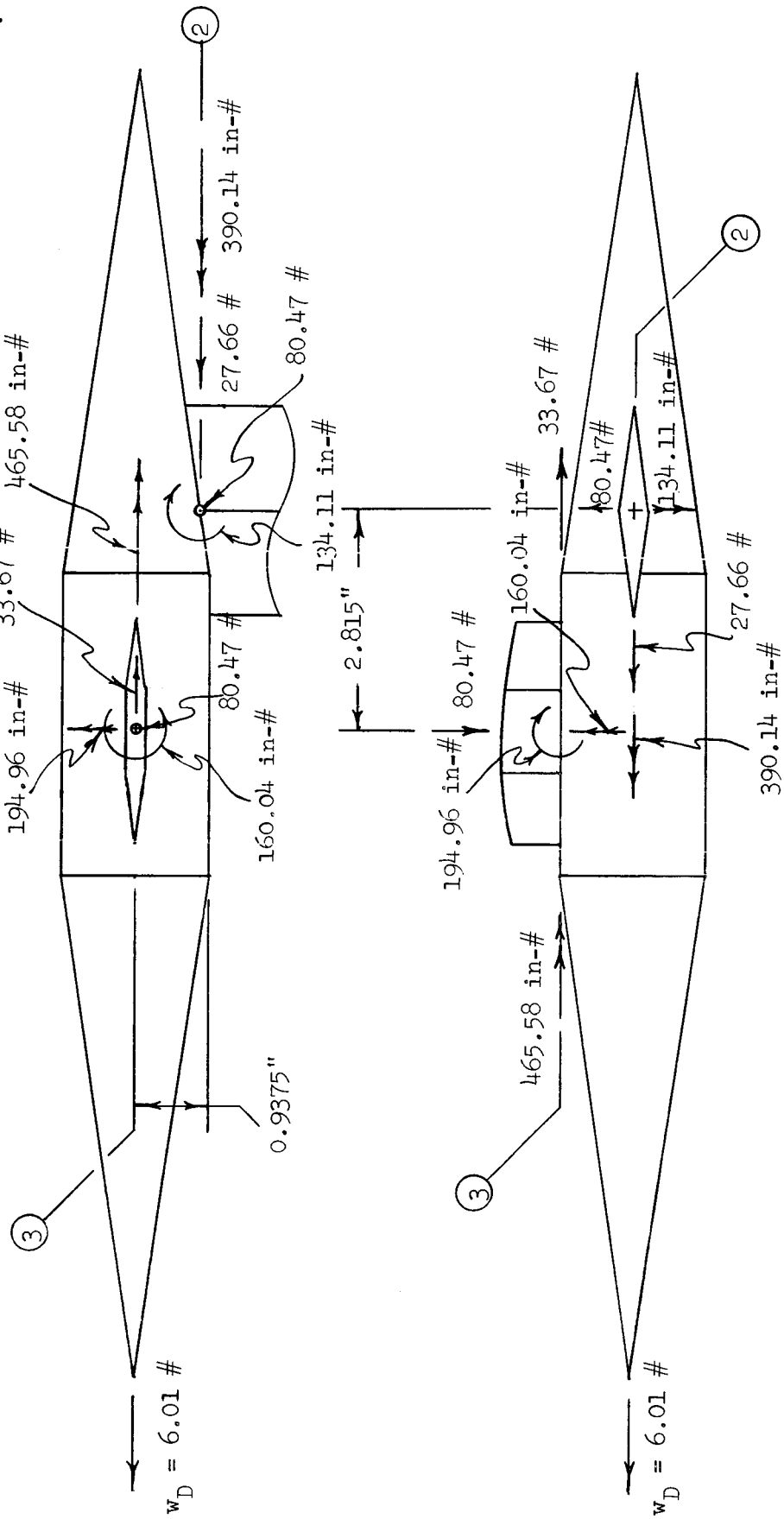
2
3
465.58 in-#
33.67 #
194.96 in-#
80.47 #
160.04 in-#
0.9375"
27.66 #
390.14 in-#
80.47 #
134.11 in-#
2.815"
w_D = 6.01 #

Section (3-4).

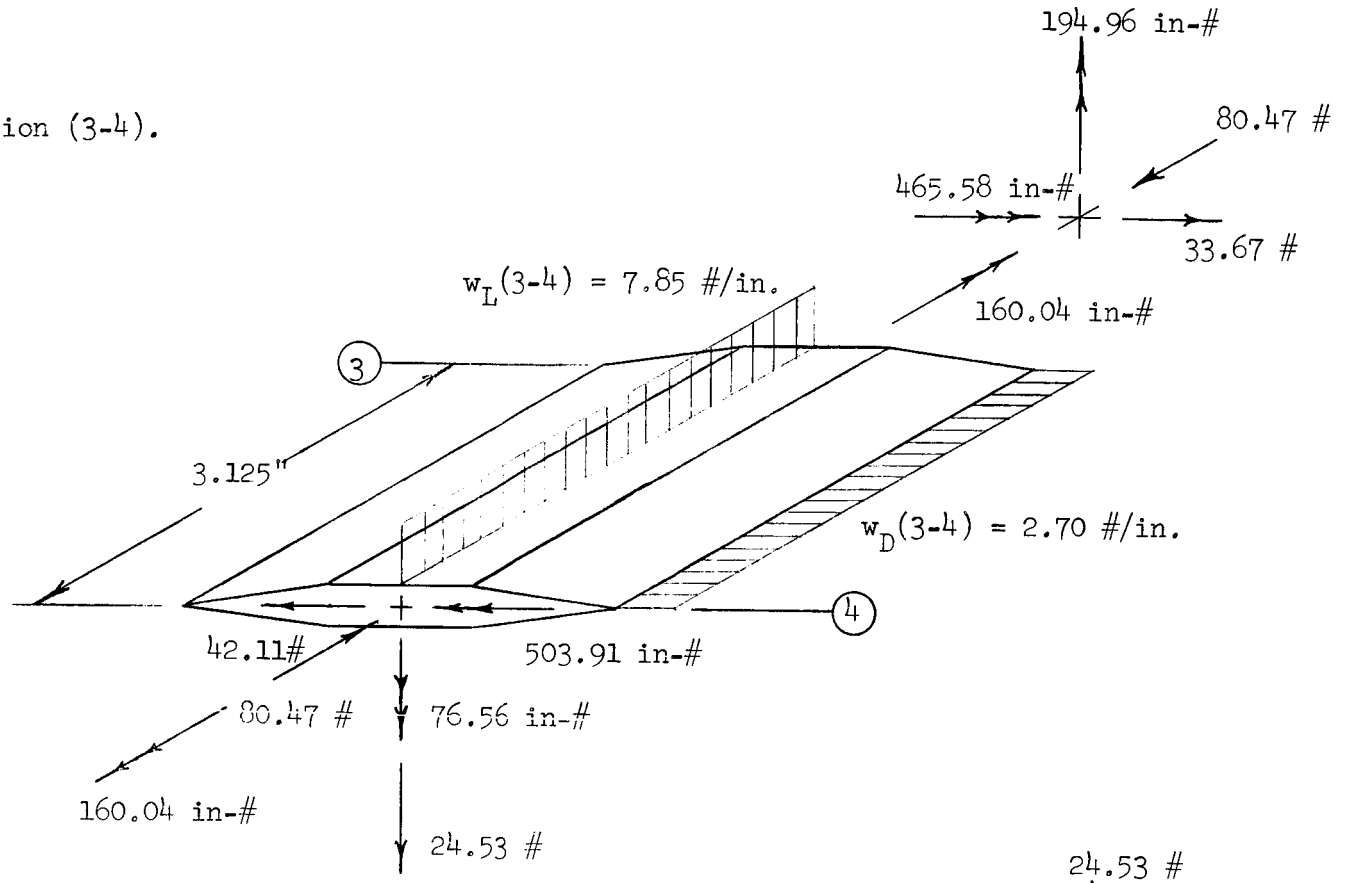

Section (4-5).

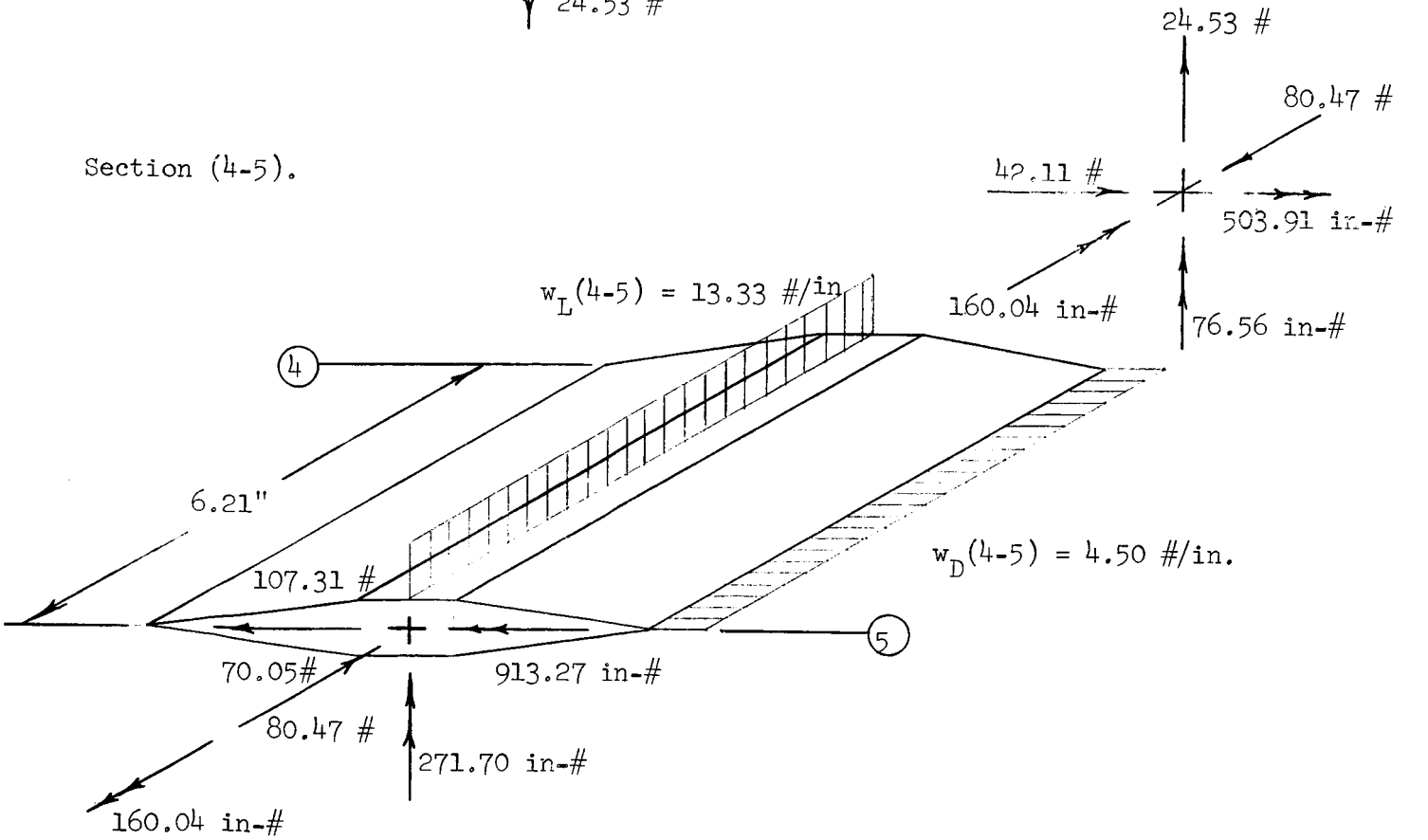

Section (5-6), (6-7).

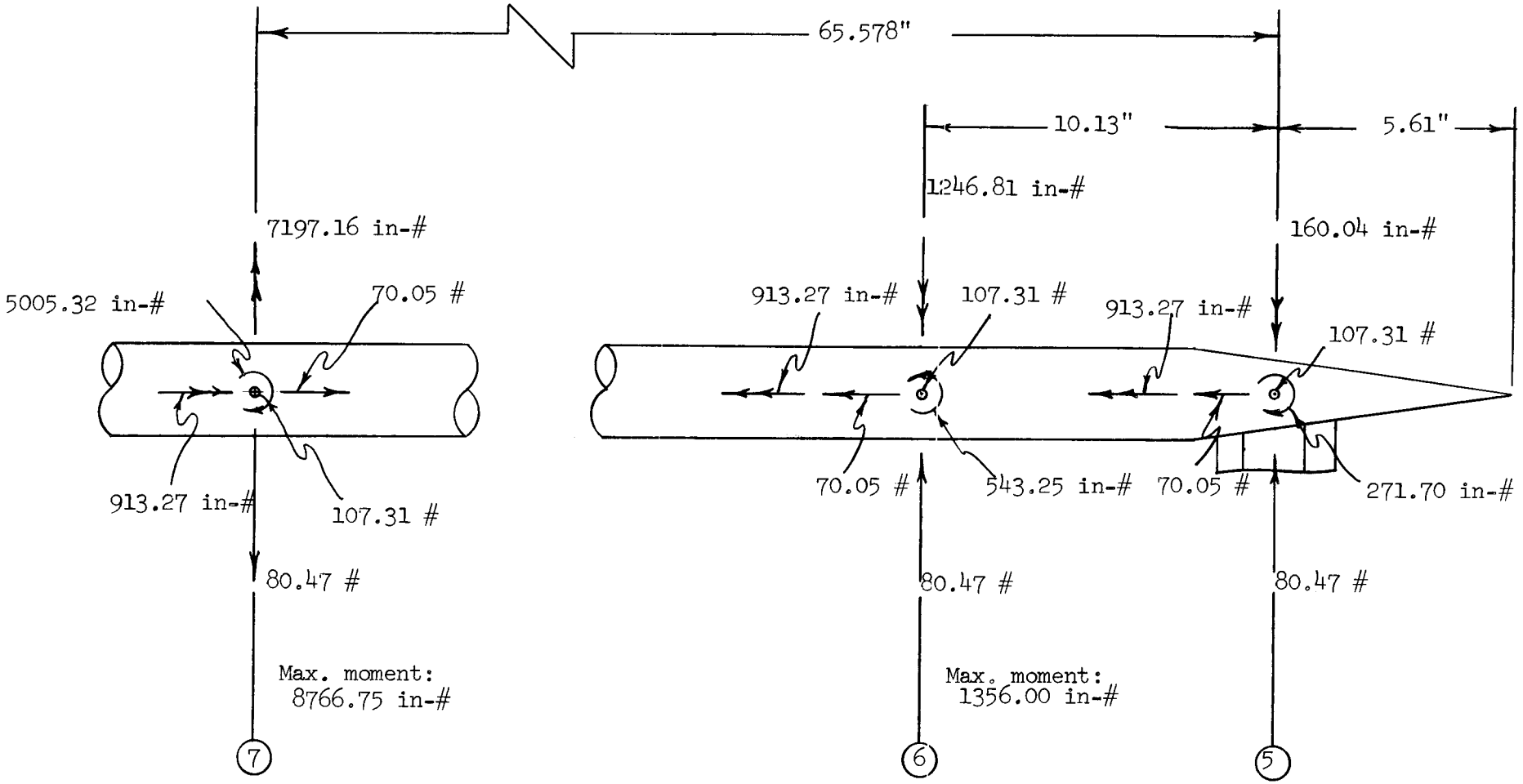

The cross-sections of the various portions of the strut are very nearly symmetrical and for simplicity have been analyzed as though they were symmetrical.

Stresses have been analyzed only in the minor directions, and therefore, the moments of inertia are needed in those directions exclusively. Further, the only strut experiencing a torque is the inboard strut, and consequently, the torsional rigidities for its sections solely are required for analysis.

The pertinent moments of inertia [23] are as follows:

Section (0-1).

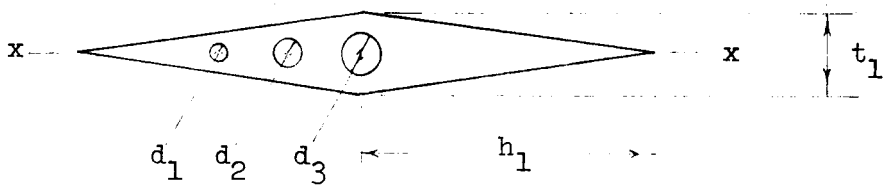

$$I_{xx} = 2\left(\frac{1}{48} t_1^3 h_1\right) - \frac{\pi}{64}\left(d_1^4 + d_2^4 + d_3^4\right)$$

where

$t_1 = 0.219$ in.

$h_1 = 0.778$ in.

$d_1 = 0.06250$ in.

$d_2 = 0.09375$ in.

$d_3 = 0.14063$ in.

Section (1-2).

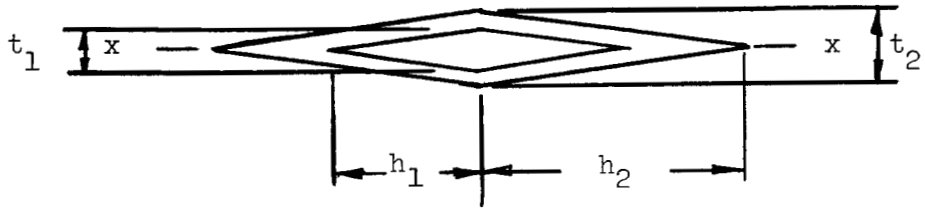

$$I_{xx} = \frac{1}{24} [t_2^3 h_2 - t_1^3 h_1]$$

where

$h_1 = 0.7785"$ $\quad$ $t_1 = 0.2200"$

$h_2 = 1.3225"$ $\quad$ $t_2 = 0.3716"$

Section (3-4).

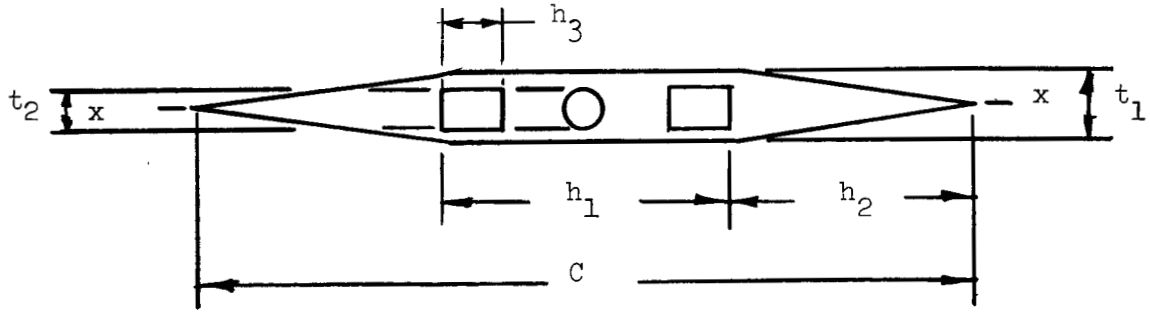

$$I_{xx} = \frac{1}{24} h_2 t_1^3 + \frac{1}{12} h_1 t_1^3 - \frac{1}{6} h_3 t_2^3 - \frac{\pi}{64} t_2^4$$

where

$C = 2.728"$ $\quad$ $h_1 = 0.950"$

$t_1 = 0.250"$ $\quad$ $h_2 = 0.889"$

$t_2 = 0.156"$ $\quad$ $h_3 = 0.281"$

Section (4-5).

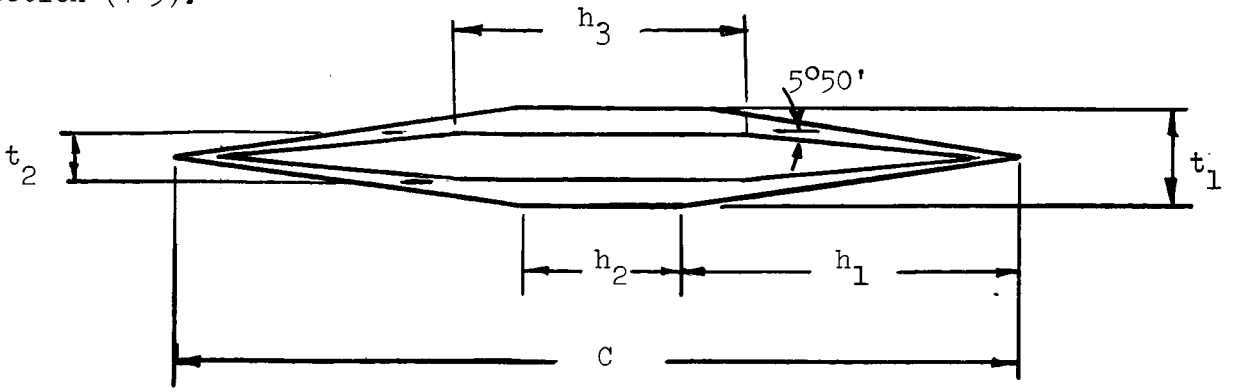

$$I_{xx} = \frac{1}{24} h_1 t_1^3 + \frac{1}{12} h_2 t_1^3 - \frac{1}{24}\left[\frac{t_2}{2} \cot (5°50')\right] t_2^3 - \frac{1}{12} h_3 t_2^3$$

where

C = 4.058 in.	h_1 = 1.7477 in.
t_1 = 0.500 in.	h_2 = 0.5625 in.
t_2 = 0.256 in.	h_3 = 0.9500 in.

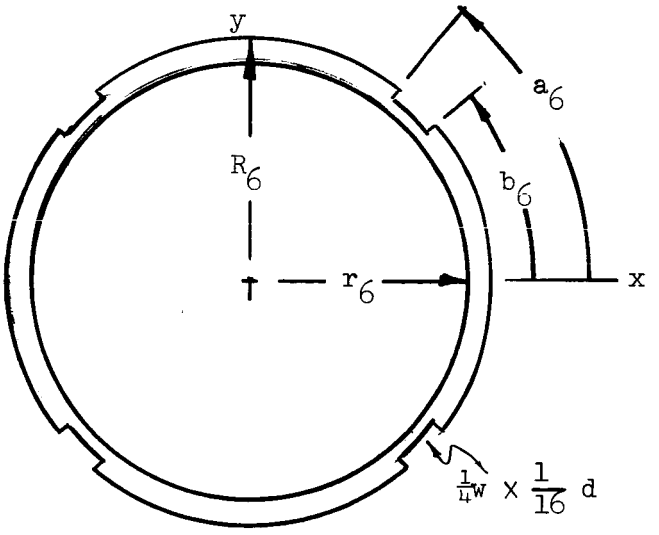

Station 6.

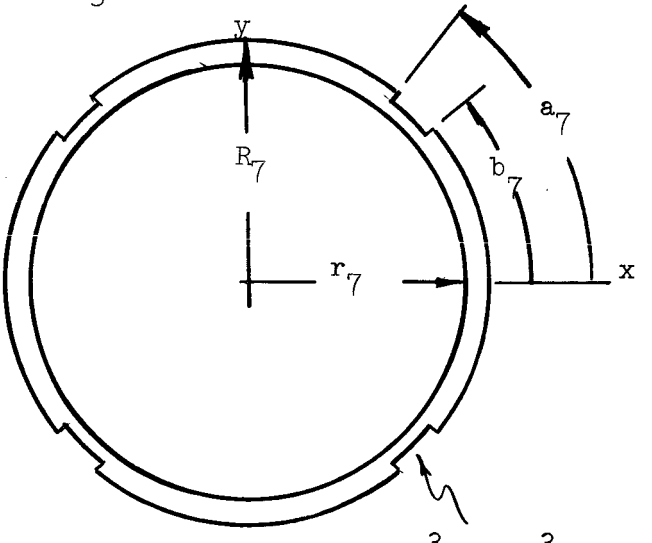

Station 7.

$$I_{xx} = I_{yy} = \frac{\pi}{4}\left[R^4 - r^4\right] - \frac{1}{2}\left[a - b\right]\left[R^4 - (\text{R-gap depth})^4\right]$$

$$J = I_{xx} + \frac{\pi}{4}\left[(\text{R - gap depth})^4 - r^4\right]$$

where

R_6 = 1.0625 in. ; r_6 = 0.9375 in. ; R_7 = 1.6875 in. ; r_7 = 1.3125 in.

a_6 = 0.9029 rad ; b_6 = 0.6676 rad ; a_7 = 0.89644 rad ; b_7 = 0.67424 rad

Mansfield [24] solves for the torsional rigidities of diamond sections; his results are given as a plot of thickness to chord ratio, t/C , versus a torsional rigidity coefficient in Fig. 9. However, implementation of this reference requires some interpretation concerning the geometry of the cross-sections of the inboard strut's components. The cross-sections are maximized and minimized as below into cylinders of double-wedge sections.

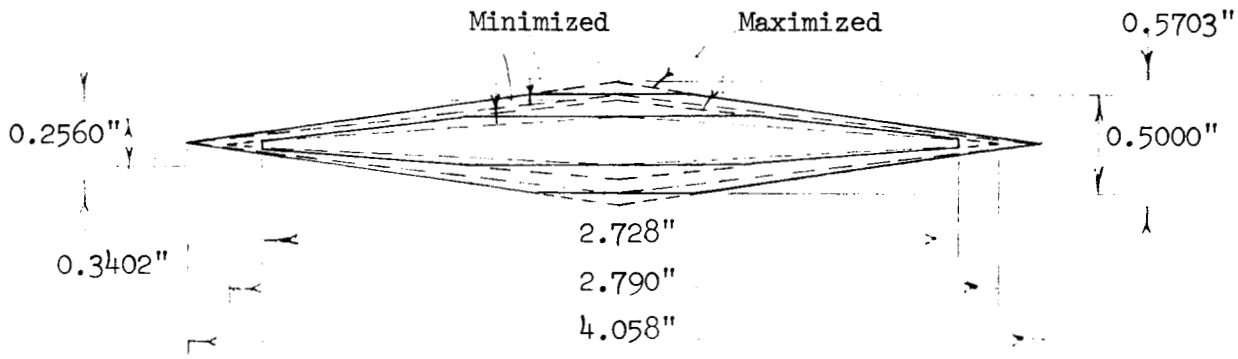

The thickness to chord ratios are determined for the modified double wedge sections of both the outer and inner cylinders; the torsional rigidity coefficients are then obtained from Fig. 9 and are tabulated below.

Diamond Section		Assumed	[t/C]	Tor. Rigidity / $[GCt^3]/12$
3-4	Outer	Maximized	0.1304	0.959
3-4		Minimized	0.0938	0.969
4-5	Outer	Maximized	0.1405	0.955
4-5		Minimized	0.1232	0.965
4-5	Inner	Maximized	0.1219	0.966
4-5		Minimized	0.0917	0.972

The average torsional rigidity coefficients become:

for the outer double-wedge section of fixed section of the inboard strut

$$\frac{0.955 + 0.965}{2} = 0.960$$

for the inner double-wedge section of fixed section of the inboard strut

$$\frac{0.966 + 0.972}{2} = 0.969$$

for the outer double-wedge section of moveable section of the inboard strut

$$\frac{0.959 + 0.969}{2} - 0.964$$

The inner portion of the moveable section of the inboard strut consists of two rectangular cutouts and a circular cutout. These cutouts are replaced by one rectangular cutout as shown below for the torsional analysis.

Now, let

$$J_i = \alpha_i \frac{c_i t_i^3}{12}$$

where

$\alpha_1 = 0.960$	$c_1 = 4.058$ in.	$t_1 = 0.500$ in.
$\alpha_2 = 0.969$	$c_2 = 2.790$ in.	$t_2 = 0.256$ in.
$\alpha_3 = 0.964$	$c_3 = 2.728$ in.	$t_3 = 0.256$ in.
$\alpha_4 = 1.000$	$c_4 = 0.950$ in.	$t_4 = 0.156$ in.

The equivalent J of section (3-4) is assumed to be the equivalent J of the averaged outer double-wedge solid section minus the equivalent

J of the assumed inner rectangular section, i.e.,

$$J_{(3-4)} = J_3 - J_4$$

Similarly, for section (4-5),

$$J_{(4-5)} = J_1 - J_2$$

The section properties are then tabulated as follows:

Section	Moment of Inertia	Equivalent J
0-1	0.000326 $in.^4$	
1-2	0.002483 $in.^4$	
3-4	0.001609 $in.^4$	0.00338 $in.^4$
4-5	0.012755 $in.^4$	0.03680 $in.^4$
5-6	0.361910 $in.^4$	0.54061 $in.^4$
6-7	3.853960 $in.^4$	6.59080 $in.^4$

With these section properties, the bending and torsional stresses are calculated using the equations

$$\sigma = \frac{M\ t/2}{I_{xx}}$$

and

$$\tau = \frac{T\ t/2}{J}$$

respectively, while the maximum stress is estimated by

$$\sigma_{max} = \frac{\sigma}{2} + \sqrt{\left(\frac{\sigma}{2}\right)^2 + \tau^2}$$

The material has the following properties:

Station 1-5: Stainless Steel Type 17-4 PH Hardened to 33-35 Rockwell C
Yield: 125,000 psi
Ultimate: 145,000 psi

Station 6-7: Stainless Steel Type 304
Yield: 35,000 psi
Ultimate: 85,000 psi

A summary of pertinent information and the safety factors for yield and ultimate stress at the various stations is given in the next tables.

Station No.	C in.	I_{xx} $in.^4$	J $in.^4$	M in.-#	T in.-#
1	0.1095	0.000326		69.14	
2	0.1858	0.002483		390.14	
3	0.1250	0.001609	0.00388	465.58	160.04
4	0.1250	0.001609	0.00388	503.91	160.04
5	0.2500	0.012755	0.0368	913.27	160.04
6	1.0625	0.36191	0.54061	1366.00	913.27
7	1.6875	3.85396	6.5908	8766.75	913.27

Station No.	σ psi	τ psi	σ_{max} psi	S. $F._y$	S. $F._u$
1	23,223		23,223	5.382	6.244
2	29,193		29,193	4.281	4.967
3	36,170	5,919	37,114	3.368	3.906
4	39,148	5,919	40,023	3.123	3.622
5	17,893	1,087	18,532	6.745	7.824
6	4,010	1,795	8,025	4.361	10.592
7	3,838	234	3,852	9.085	22.065

It is desirable to obtain a safety factor of 3.0 for yield and of 5.0 for ultimate stress. It is seen that all stations are satisfactory with regard to yield but that stations 3 and 4 are below the desirable safety factor for ultimate stress.

Since the loading at all stations is a linear function of the dynamic pressure and the loadings are zero for $q = 0$, the maximum dynamic pressure corresponding to a safety factor of 5 for ultimate stress at the critical station 4 becomes

$$q_{max} = \frac{3.622}{5} \times 1800 = 1303 \text{ psf}$$

with all airfoils subjected to a three degree angle-of-attack.

A facsimile of the motor pod brazed joint at station 3 has been experimentally tested with the following results. With the motor pod fixed, a) a tensile force of $\approx$ 10,000 lbs. was required to pull the strut out of the pod, and b) a bending moment of $\approx$ 2970 lbs.-in. at station 3 was required to fail the joint. Since the maximum estimated moment is 465.38 lb.-in. (see page 42), a safety factor of ≈ 6.4 seems available.

3) Static and total pressure sensors. A proper design of the geometry for the static and total pressure sensors must take into consideration the physical characteristics of the flow which is to be investigated. The flow in question is that of a turbulent boundary layer of variable thickness (1/2 to 2-inch depth) on a wavy wall in the low supersonic speed range. The wave amplitude to boundary layer thickness ratio is very small so that essentially the capabilities of the sensors must be the same as for conventional boundary layer survey instruments in this speed range. In any case, accurate measurements in the very near vicinity of the wall, particularly those of static pressure, are not considered possible with a general-purpose survey instrument due to wall interference effects which are difficult to analyze and due to misalignment of the probe with the flow in the case of the wavy wall.

In the present case, the design relies on available literature investigating the possible causes of inaccuracies of logical geometry probes for sensing static and total pressures. While such probes are used extensively, no detailed investigation has been found which deals with design for optimum performance.

Details of the selected design of the static and total pressure sensors are shown in Fig. 10 and 11. Each sensor together with its stiffener and plastic support is identical and interchangeable on the supporting strut as shown in Fig. 10 except for details of its "sensing" end which are shown in Fig. 11. Insofar as measurement capabilities are concerned, the pertinent dimensions are the tube diameters, both of which are 0.030 inches with unsupported lengths beyond the stiffeners of 1.75 inches. The static pressure probe consists of a 4^{o} cone at its tip followed by four 0.010 inch holes with 90^{o} spacing around the tube, these holes being located 15 diameters behind the cone shoulder. The total pressure probe is flattened at its tip so as to present a total thickness of 0.007 inches with an inside opening 0.003 inches in height. None of these dimensions are deemed critical.

Evidence to support the conclusion that these probes will provide accurate results in the experiment under consideration is given in the literature. Of primary importance is the selection of the probe diameters; Wilson and Young [25] indicate that the aerodynamic interference of pitot tubes of diameters less than six per cent of the boundary layer thickness has negligible effect on turbulent boundary layer characteristics at a freestream Mach number of 2. This result, if correct, allows use of the present probes in boundary layers at least as thin as 1/2 inch.

The sensitivity of the probes to errors induced by misalignment with the flow have also been considered. Strack [26] finds that carefully flattened total pressure probes that provide a symmetrically placed hole area which is a reasonable fraction of the total frontal area will yield errors of the order of only one per cent at angles-of-attack as high as 10°. Hasel and Coletti [27] indicate from fairly extensive tests that at low supersonic Mach numbers a static pressure probe, similar in design to the present probe, with orifices located at least eight diameters behind the end of the nose section should provide fairly accurate static pressure measurements at angles-of-attack of $\pm 3^{\circ}$ within an error of approximately three per cent.

VII. CONCLUDING REMARKS

The initial results of the analysis for predicting in low supersonic flow the flutter boundaries for a very low aspect ratio panel are promising and a more extensive verification of results with previously derived information is required. It is, therefore, recommended that this analysis be continued under NASA Contract NAS8-20100 titled "Experimental Research on Panel Flutter Aerodynamics."

The half amplitude to wave length ratio for the stationary two-dimensional wavy wall models should be approximately 5×10^{-3} at $M = 1.35$ to avoid the effects of more linearity in the pressure distribution and thus circumvent separation and shock waves. It is anticipated that this criteria can be somewhat relieved for the three-dimensional models.

The stress analysis of the boundary layer probe indicates a safety factor of 3.123 for yield and 3.622 for ultimate stress when all aerodynamic surfaces are subjected to a three degree angle-of-attack and the dynamic pressure is 1800 psf. To obtain a safety factor of five for ultimate stress, the dynamic pressure should be reduced to 1303 psf.

REFERENCES

1. Fung, Y. C., Some Recent Contributions to Panel Flutter Research, AIAA Journal, Vol. 1, No. 4, pp. 898-909, April, 1963.

2. Cunningham, H. J., Analysis of the Flutter of Flat Rectangular Panels on the Basis of Exact Three-Dimensional, Linearized Supersonic Potential Flow, AIAA Journal, Vol. 1, No. 8, pp. 1795-1801, August, 1963.

3. Kordes, E. E., Tuorilla, W. J. and Guy, L. D., Flutter Research on Skin Panels, NASA TN D-451, 1960.

4. Lock, M. H. and Fung, Y. C., Comparative Experimental and Theoretical Studies of the Flutter of Flat Panels in a Low Supersonic Flow, AFOSR TN 670, GALCIT, California Institute of Technology, May, 1961.

5. Dowell, E. H. and Voss, H. M., Experimental and Theoretical Panel Flutter Studies with Mach Number Range of 1.0 to 5.0 (Unclassified Title, Confidential Report), ASD-TDR-63-449, December, 1963.

6. Ketter, D. J. and Voss, H. M., Panel Flutter Analyses and Experiments in the Mach Number Range of 5.0 to 10.0 (Unclassified Title, Confidential Report), FDL-TDR-64-6, March, 1964.

7. Asher, G. W. and Brown, A. W., Experimental Studies of the Unsteady Aerodynamics of Panels at or Near Flutter with a Finite Boundary Layer, Mach Number 1 to 10, RTD-TDR-63-4268, December, 1964.

8. Zeydel, E. F. E., Large Deflection Panel Flutter, AFOSR Tech. Note 1952, January, 1962.

9. Zeydel, E. F. E. and Kobett, D. R., The Flutter of Flat Plates with Partially Clamped Edges in the Low Supersonic Region, AIAA Journal, Vol. 3, No. 1, pp. 17-22, January, 1965.

10. Miles, J. W., On the Aerodynamic Stability of Thin Panels, Journal of the Aeronautical Sciences, Vol. 23, No. 8, pp. 771-780, August, 1956.

11. Kobett, D. R. and Zeydel, E. F. E., Research on Panel Flutter, NASA TN D-2227, November, 1963.

12. McClure, J. D., On Perturbed Boundary Layer Flows, M.I.T. Fluid Dynamics Research Laboratory, Report No. 62-2, Massachusetts Institute of Technology, June, 1962.

13. Dowell, E. H., The Flutter of Very Low Aspect Ratio Panels, AFOSR 64-1723, ASRL 112-2, July, 1964.

14. Luke, Y. L. and St. John, A. P., Supersonic Panel Flutter, WADC Tech. Report 57-252, July, 1957.

REFERENCES (Concluded)

15. Erdelyi, A., et al, Tables of Integral Transforms, Vol. 1, McGraw-Hill, 1954.

16. Hedgepeth, John M., Budiansky, B. and Leonard, R. W., Analysis of Flutter in Compressible Flow of a Panel on Many Supports, Journal of the Aeronautical Sciences, Vol. 21, No. 7, p. 485, July, 1954.

17. Shapiro, A. H., The Dynamics and Thermodynamics of Compressible Fluid Flow, Vol. I, p. 561, Ronald Press, 1953.

18. Griffith, W., Shock Tube Studies of Transonic Flow Over Wedge Profiles, Journal of the Aeronautical Sciences, Vol. 19, No. 4, p. 249, 1952.

19. Liepmann, H. W. and Bryson, A. E., Jr., Transonic Flow Past Wedge Sections, Journal of the Aeronautical Sciences, Vol. 17, No. 12, p. 745, 1950.

20. Guderley, G. and Yoshihara, H., Two-Dimensional Unsymmetric Flow Patterns at Mach Number 1, Journal of the Aeronautical Sciences, Vol. 20, No. 11, p. 757, 1953.

21. Vincenti, W. F., Dugan, D. W. and Phelps, E. R., An Experimental Study of the Lift and Pressure Distribution on a Double-Wedge Profile at Mach Numbers Near Shock Attachment, NACA TN 3225, 1954.

22. Drougge, G., Some Measurements on Bodies of Revolution at Transonic Speeds, 9th International Congress of Applied Mechanics, 1956, Proceedings, Vol. 2.

23. Miller, F. E. and Doeringsfeld, H. A., Mechanics of Materials, International Textbook Company, p. 455, 1955.

24. Mansfield, E. H., The Torsional Rigidity of Solid Cylinders of Double-Wedge Section, Reports and Memoranda No. 2959, January, 1954.

25. Wilson, R. E. and Young, E. C., Aerodynamic Interference of Pitot Tubes in a Turbulent Boundary Layer at Supersonic Speed, Applied Physics Lab, John Hopkins University, Report CF-1351, 1949.

26. Strack, S. L., Supersonic Pitot Tube Measurements at an Angle of Attack, AIAA Journal, Vol. 2, No. 4, p. 778-779.

27. Hasel, L. E. and Coletti, D. E., Investigation of Two Pitot-Static Tubes at Supersonic Speeds, NACA RM L8102, 1948.

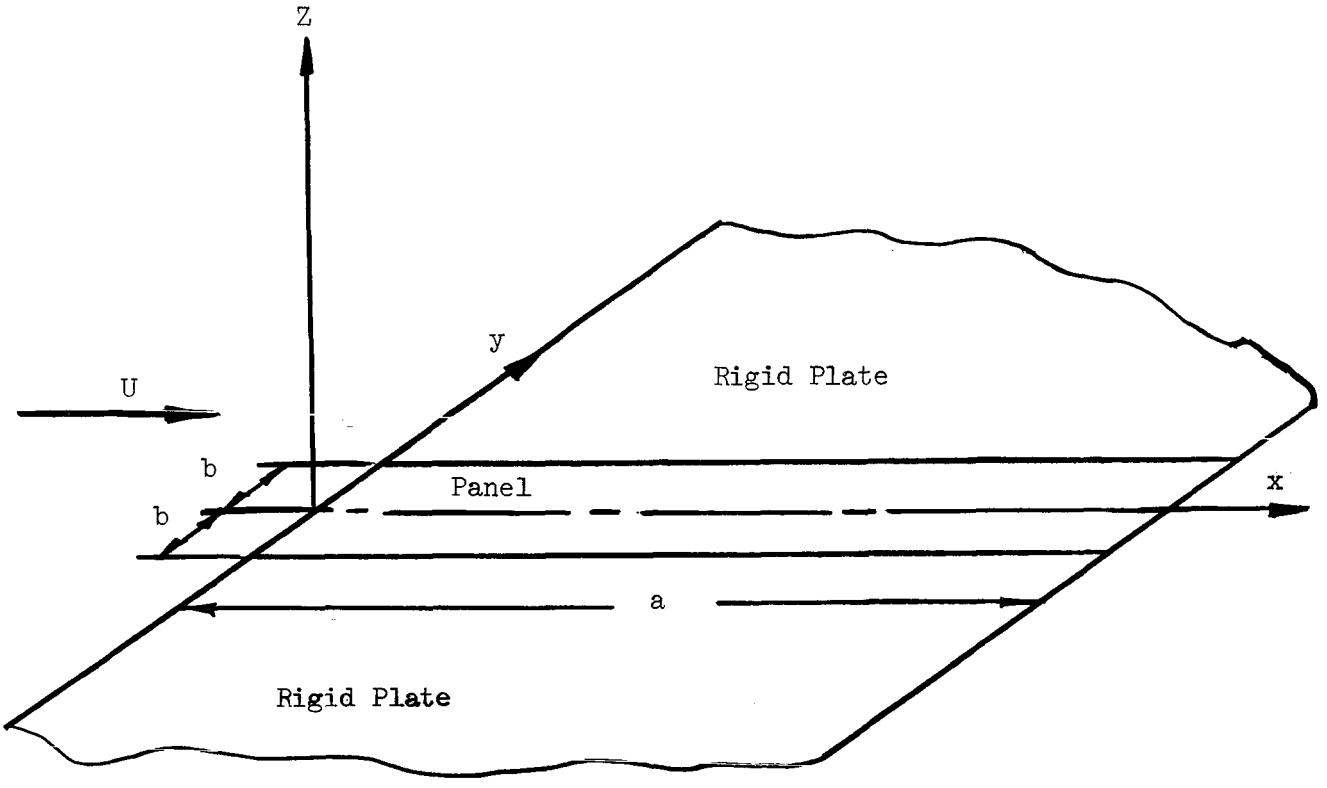

Fig. 1. Panel Configuration

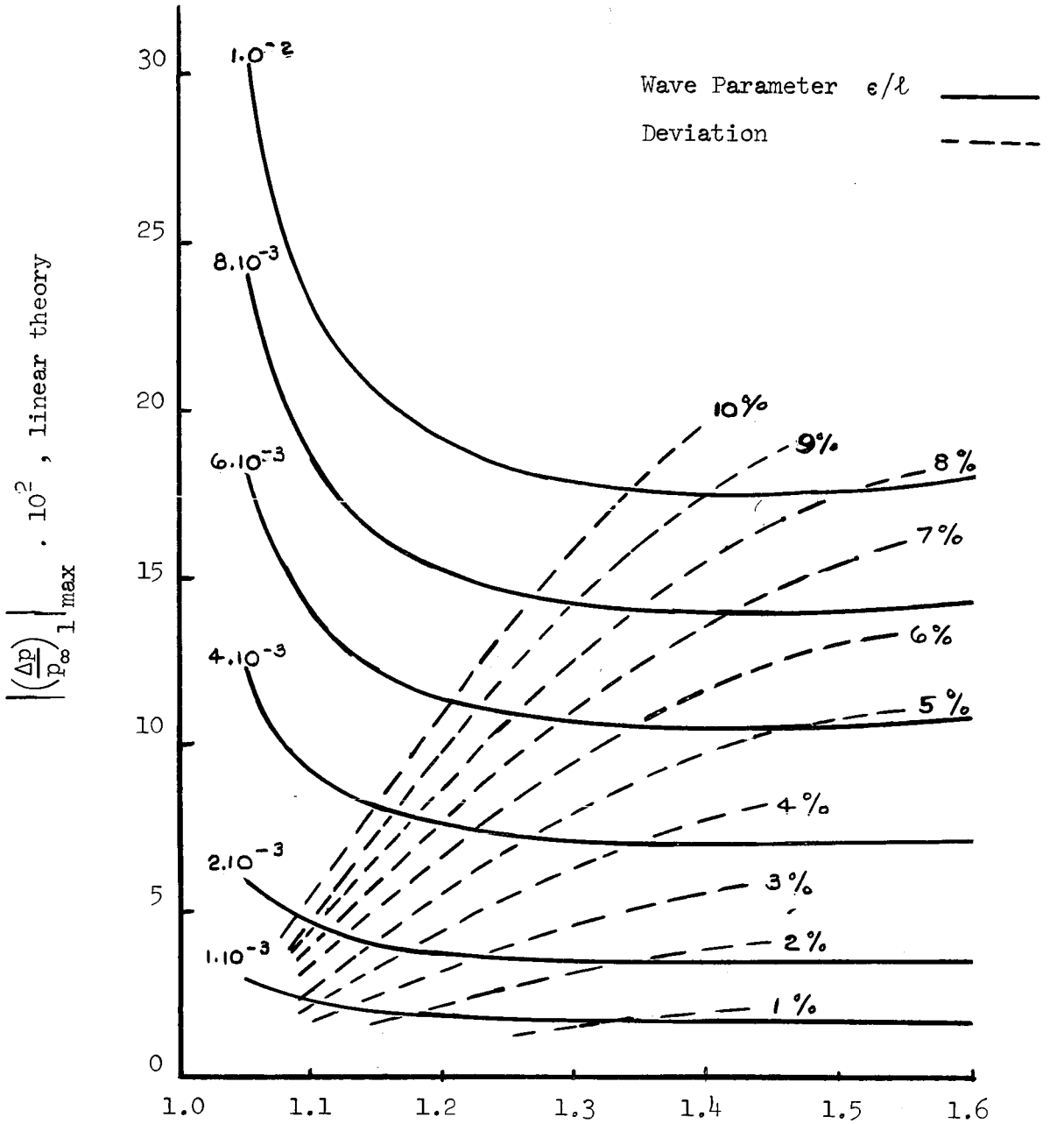

Fig. 2. Pressure Difference and Deviation

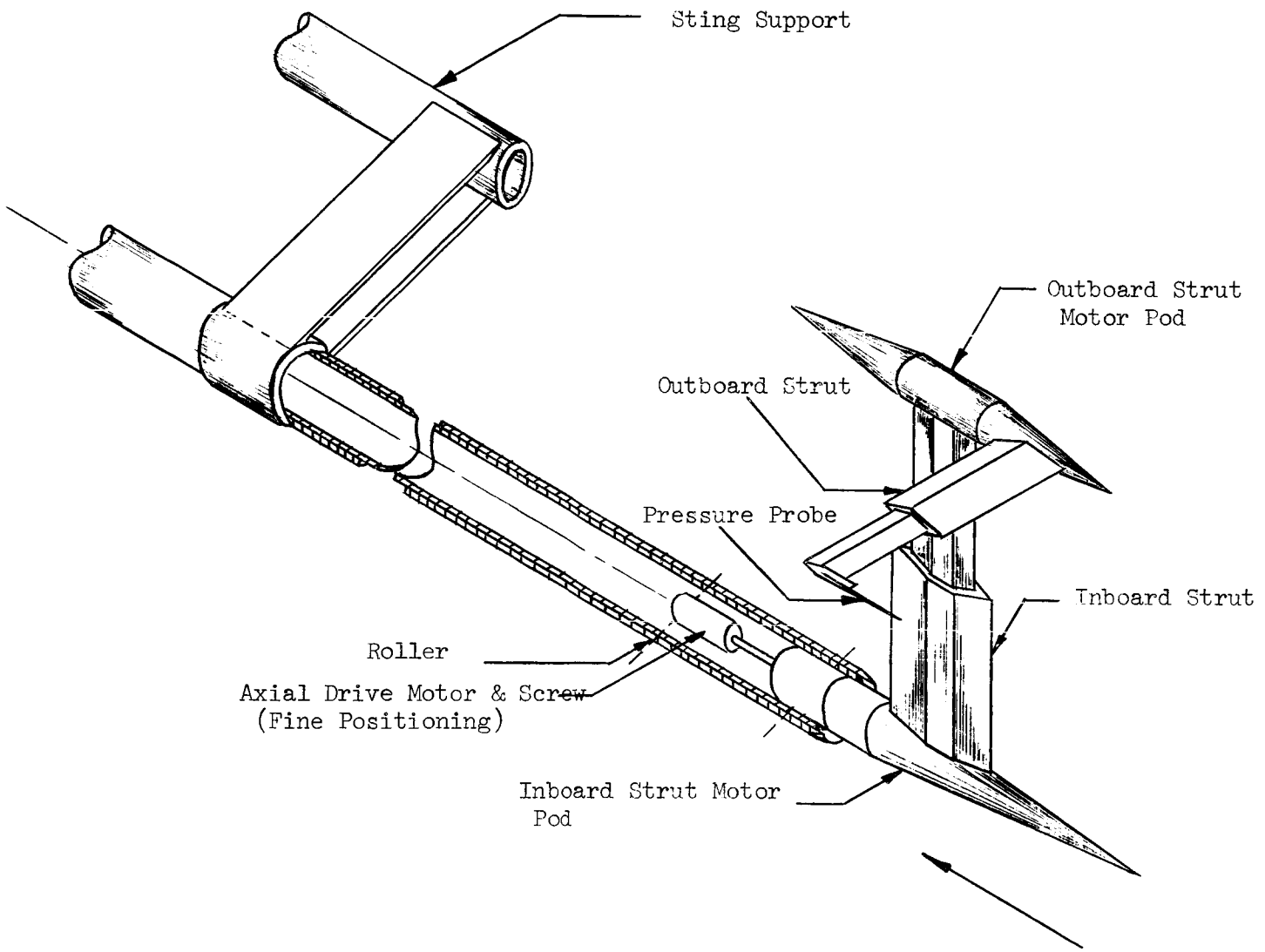

Fig. 3. Probe Mechanism

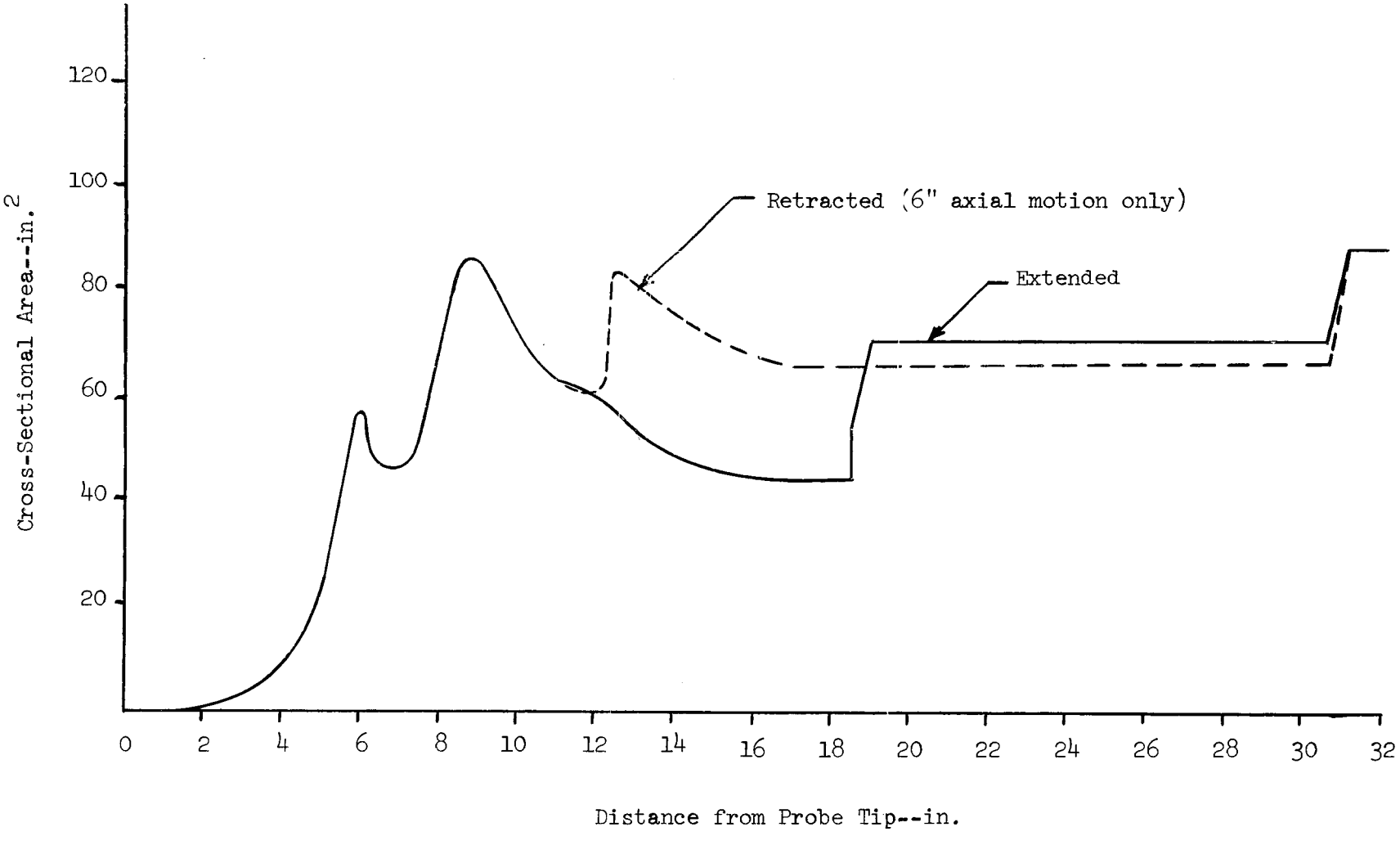

Fig. 4. Cross-Sectional Area of Mechanism vs. Distance From Probe Tip

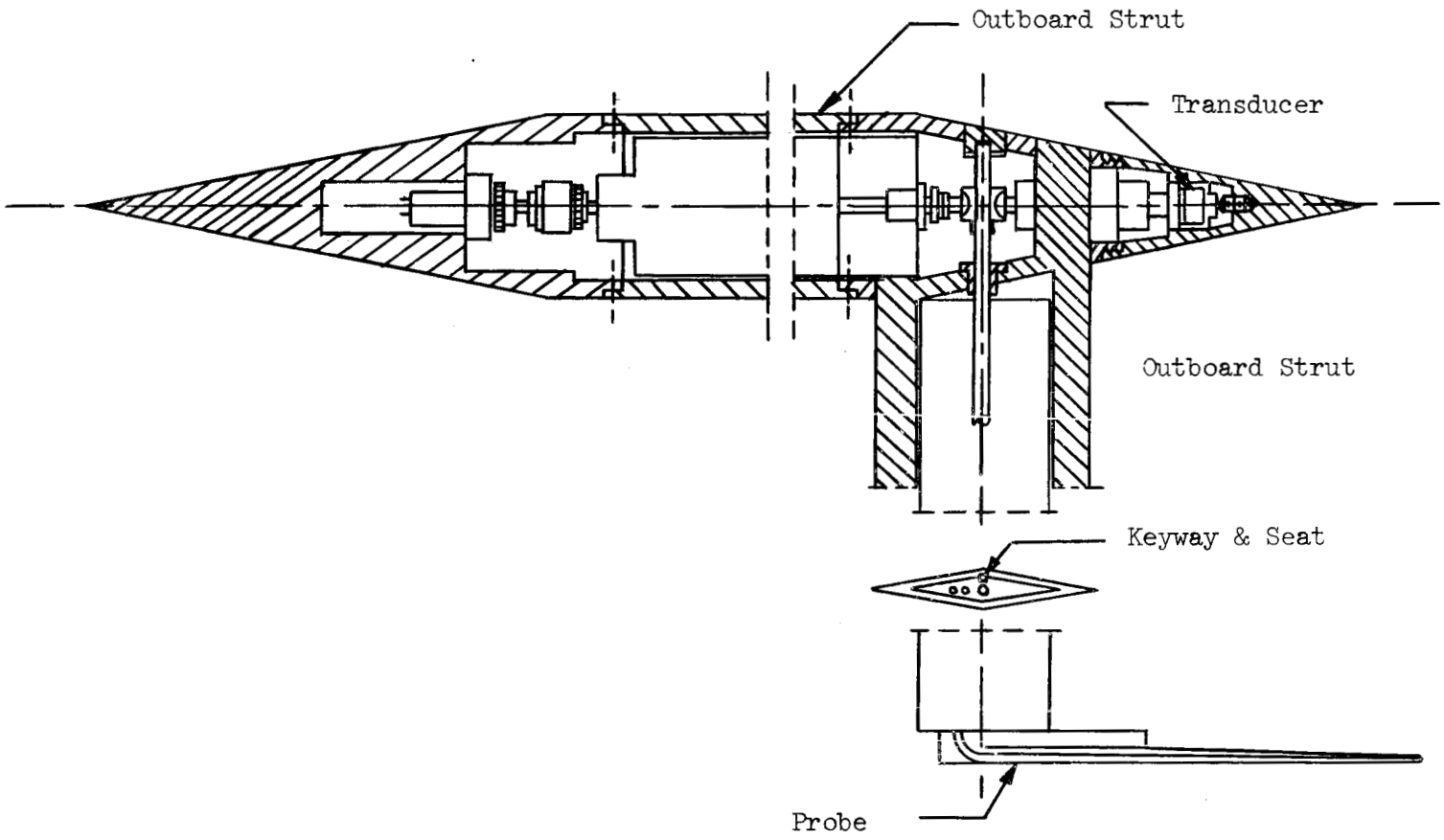

Fig. 5. Outboard Strut-Motor Pod Assembly

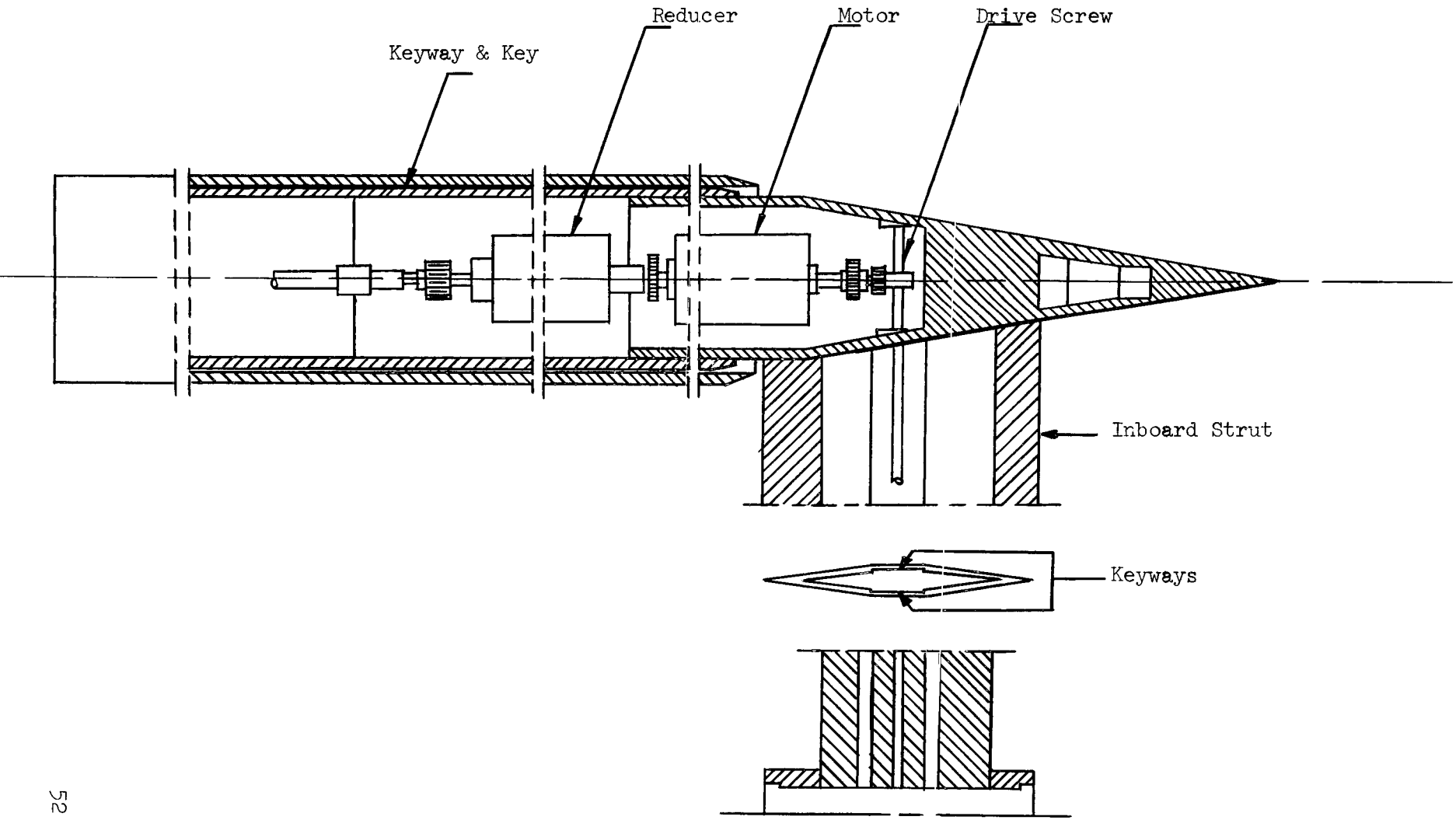

Fig. 6. Inboard Strut-Motor Pod Assembly

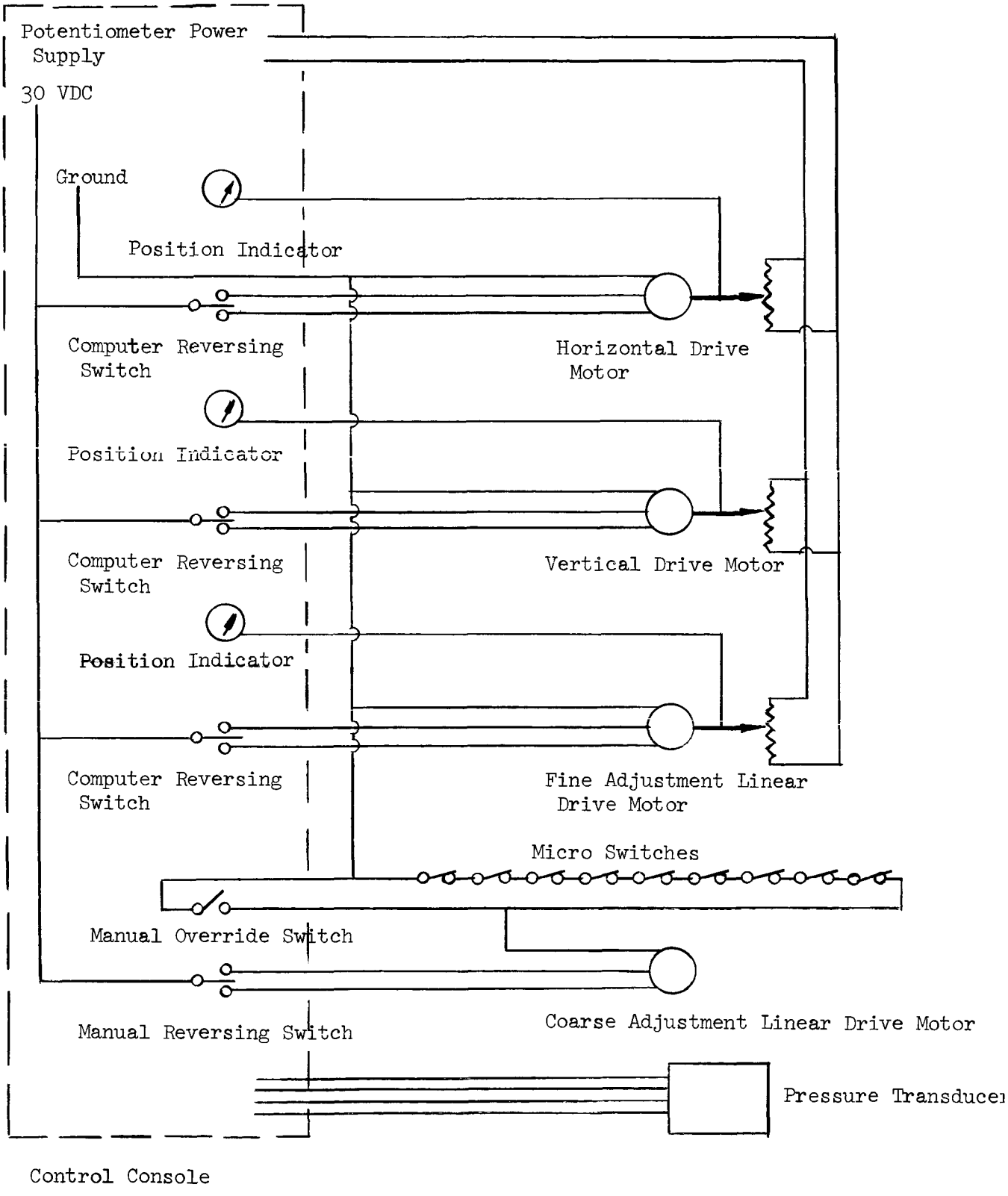

Fig. 7. Schematic of Electrical Circuitry of Sting-Strut Assembly

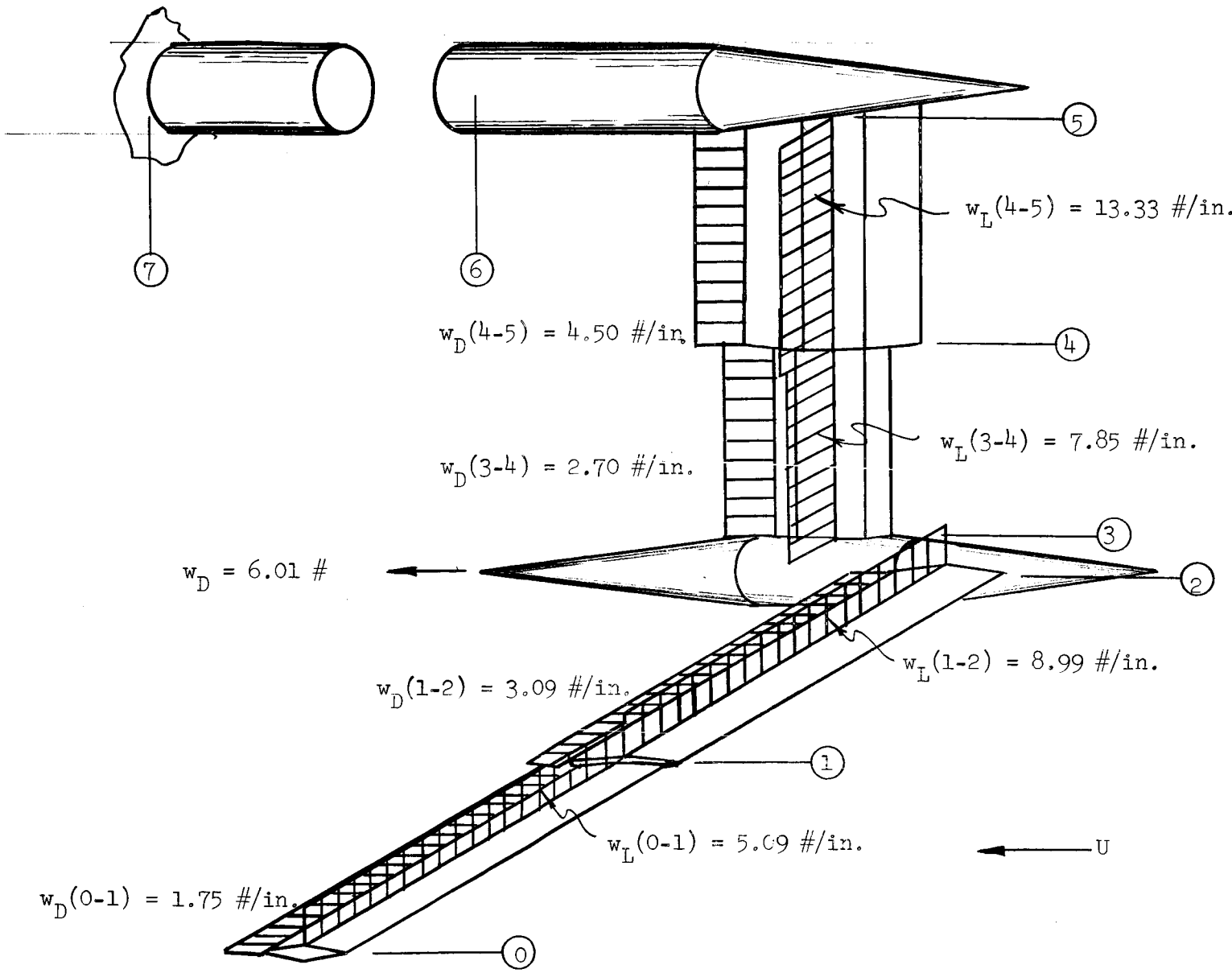

Fig. 8. Boundary Layer Probe Support Loading.

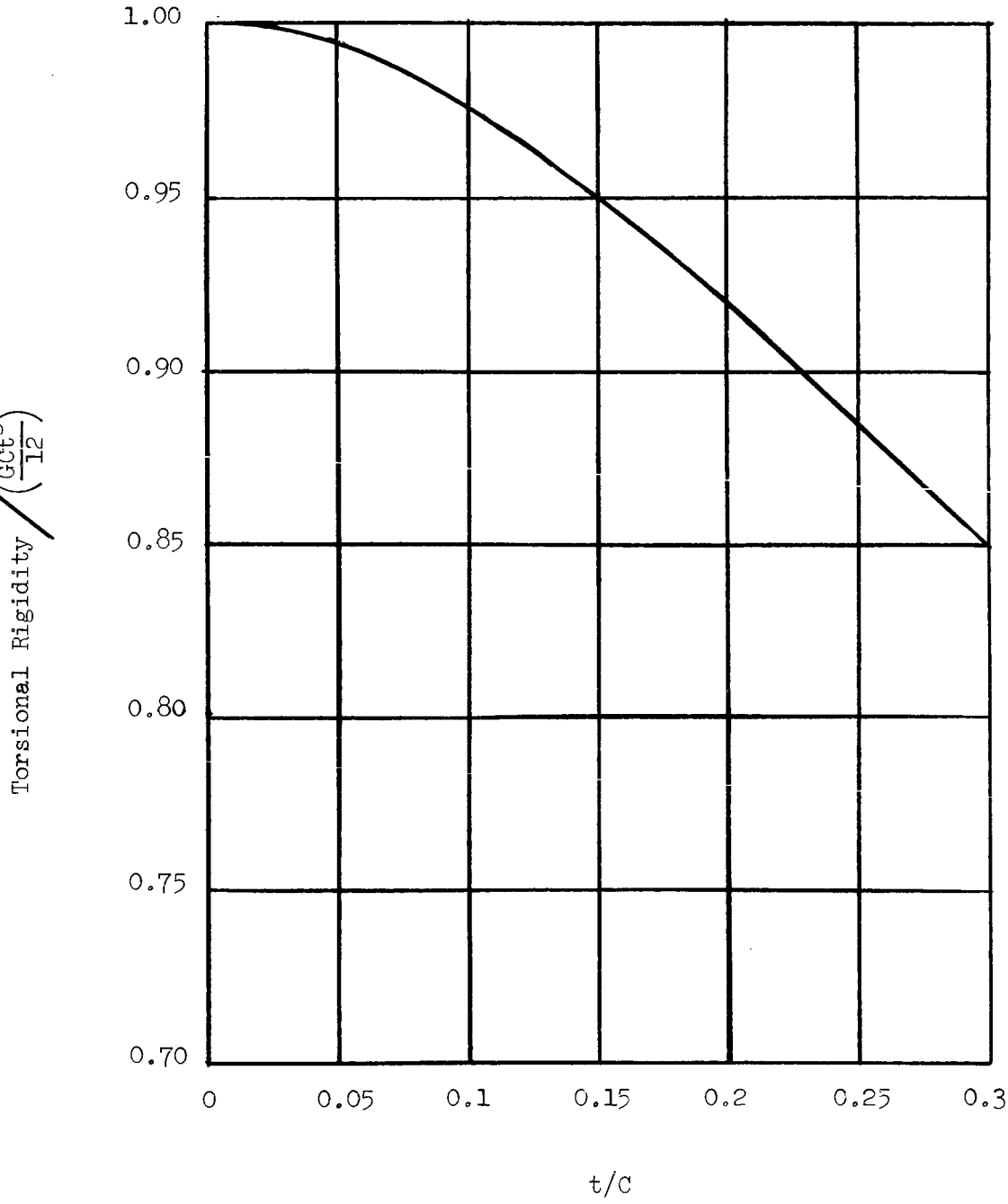

Fig. 9. Torsional Rigidity Coefficients Versus t/C Ratios [24]

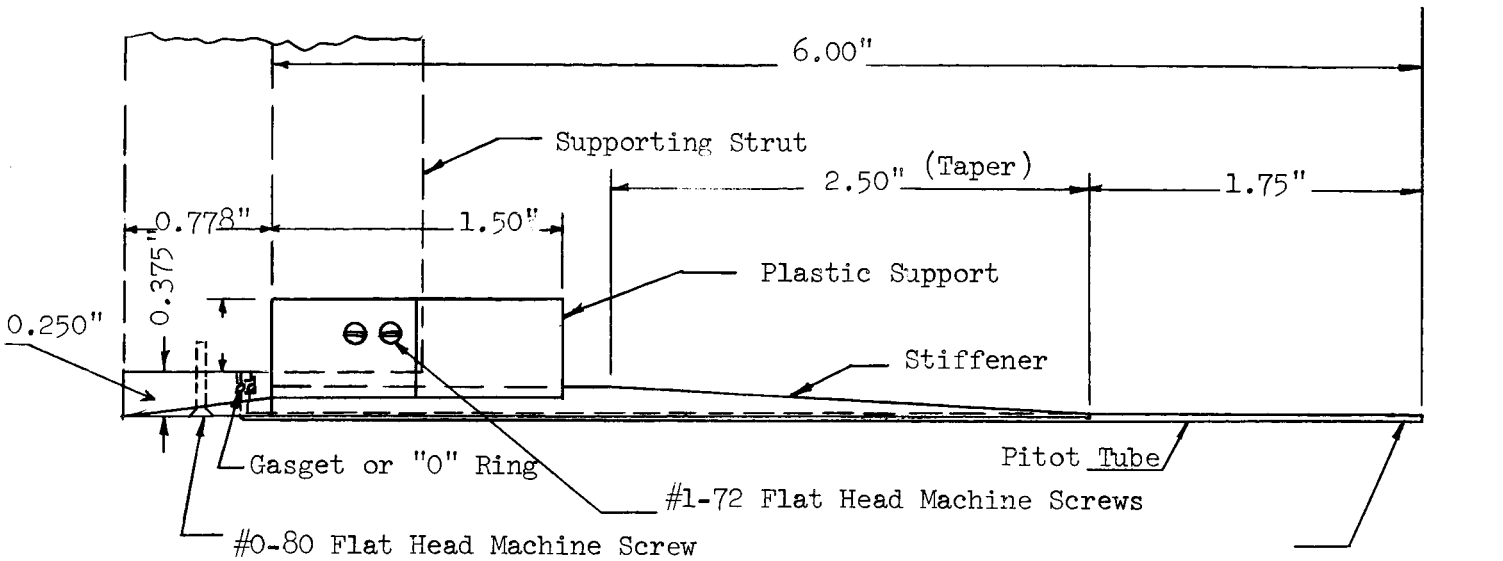

Top View

See following plate for details of pitot tube ends.

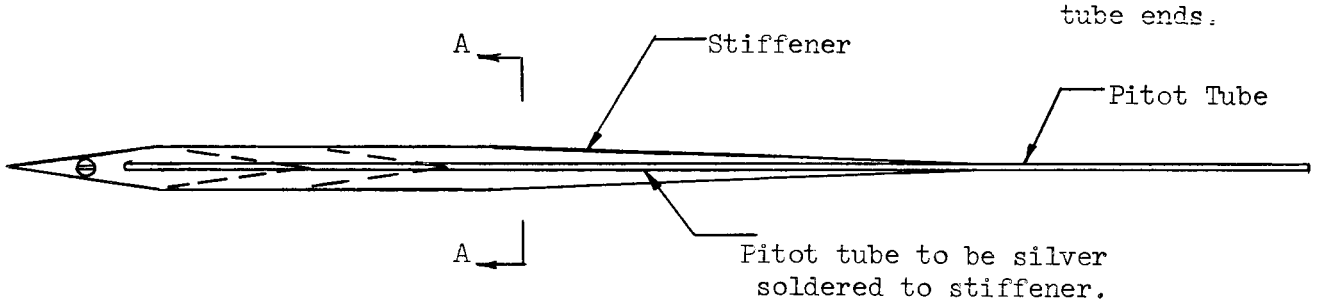

End View

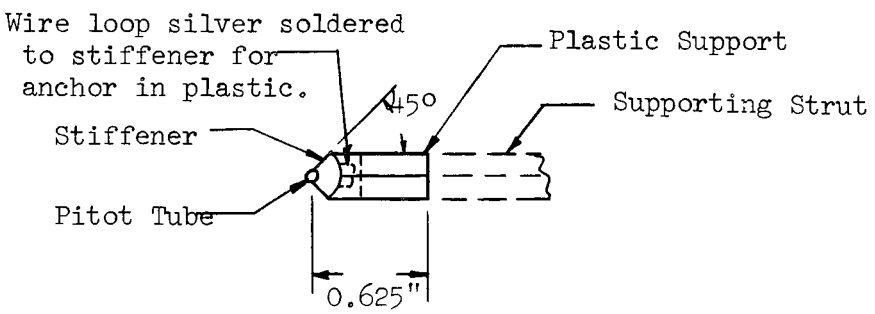

Section "AA"

Fig. 10. Static and Total Pressure Pitot Tube Supports

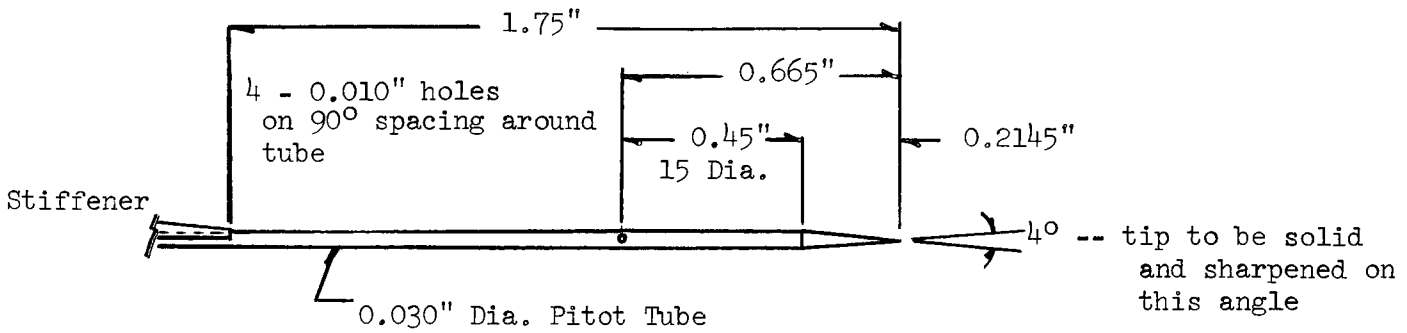

Static Pressure Tube End

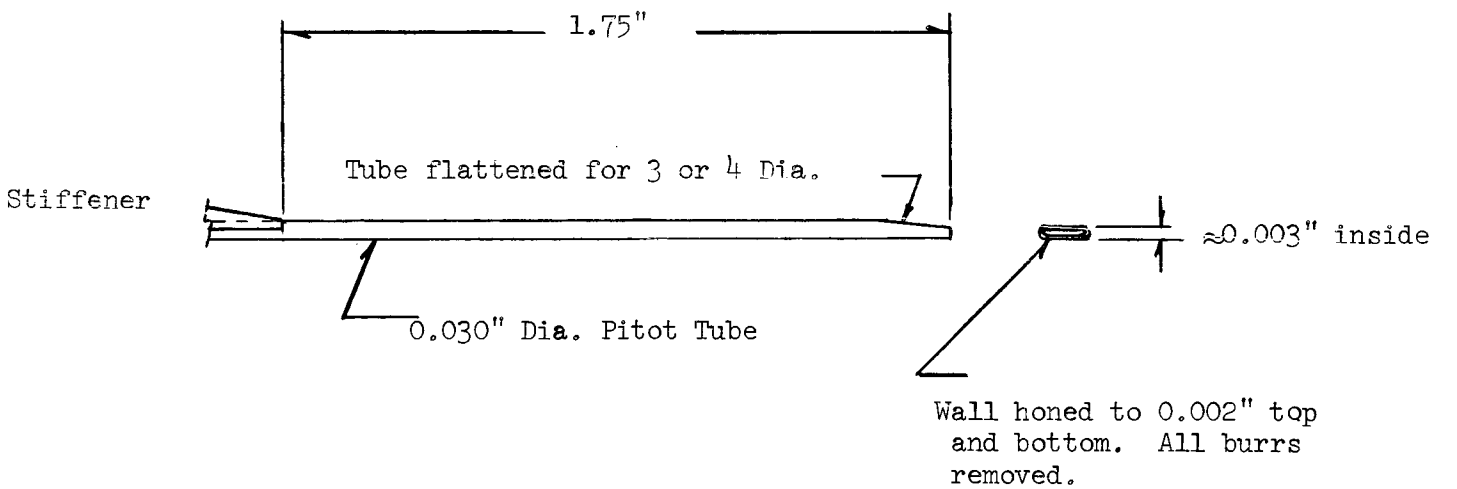

Total Pressure Tube End

Fig. 11. Total and Static Pressure Tube End